AD NUMBER

AD235971

NEW LIMITATION CHANGE

TO

Approved for public release, distribution unlimited

FROM

Distribution authorized to U.S. Gov't. agencies only; Administrative/Operational Use; MAR 1960. Other requests shall be referred to Air Force Cambridge Research Center, Hanscom AFB, MA.

AUTHORITY

afcrl ltr 3 nov 1971

UNCLASSIFIED

AD 235971

DEFENSE DOCUMENTATION CENTER

FOR

SCIENTIFIC AND TECHNICAL INFORMATION

CAMERON STATION ALEXANDRIA, VIRGINIA

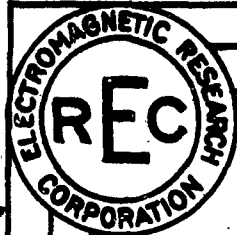# UNCLASSIFIED

DISCLAIMER NOTICE

THIS DOCUMENT IS BEST QUALITY PRACTICABLE. THE COPY FURNISHED TO DTIC CONTAINED A SIGNIFICANT NUMBER OF PAGES WHICH DO NOT REPRODUCE LEGIBLY.

AFCRC-TR-60-127

INVESTIGATIONS OF GROUND CLUTTER AND GROUND SCATTERING

by

Martin Katzin

Edward A. Wolff

Joel C. Katzin

Final Report
on
Contract AF19(604)-5198

Prepared for
ELECTRONICS RESEARCH DIRECTORATE
AIR FORCE CAMBRIDGE RESEARCH CENTER
AIR RESEARCH AND DEVELOPMENT COMMAND
BEDFORD, MASSACHUSETTS

ASTIA

MAY 6 1960

TIPDR Q

Report No. CRC-5198-4
March 15, 1960

ELECTROMAGNETIC RESEARCH CORPORATION

SHERATON BUILDING, 711-14ᵀᴴ ST., N. W.

WASHINGTON 5, D. C.

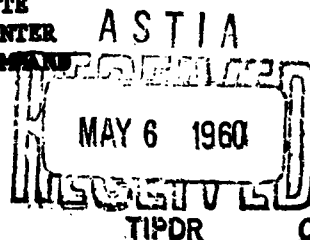INVESTIGATIONS OF GROUND CLUTTER AND GROUND SCATTERING

by

Martin Katzin

Edward A. Wolff

Joel C. Katzin

Final Report
on
Contract AF19(604)-5198

Prepared for
ELECTRONICS RESEARCH DIRECTORATE
AIR FORCE CAMBRIDGE RESEARCH CENTER
AIR RESEARCH AND DEVELOPMENT COMMAND
BEDFORD, MASSACHUSETTS

ELECTROMAGNETIC RESEARCH CORPORATION

SHERATON BUILDING, 711-14ᵀᴴ ST., N. W.

WASHINGTON 5, D. C

Report No. CRC-5198-4
March 15, 1960

Requests for additional copies by Agencies of the
Department of Defense, their contractors, and other
Government agencies should be directed to the

Armed Services Technical Information Agency
Arlington Hall Station
Arlington 12, Virginia

Department of Defense contractors must be established
for ASTIA services or have their "need-to-know" certi-
fied by the cognizant military agency of their project
or contract.

All other persons and organizations should apply to the

U. S. Department of Commerce
Office of Technical Services
Washington 25, D. C.

Abstract

The physical mechanisms which are of importance in ground clutter are discussed, and ground clutter measurements are shown which reveal the presence of these mechanisms. The significance and properties of the radar length tensor (or polarization matrix) are pointed out. The radar length tensor for small circular disks is determined, and curves are shown for certain ranges of aspect. These are used to explain some previously unexplained horizontal/vertical and cross-polarization characteristics of sea clutter.

Methods for measuring the radar length tensor are discussed, and typical coherent radar systems for ground scattering measurements are described. A new calibration technique for coherent radars is described w' .ch allows ground scattering measurements to be placed on a quantitative basis.

v

1. INTRODUCTION.

The aims of the research conducted under the present contract were

(1) to conduct research in the field of ground clutter and associated ground scattering problems, including extensions of the basic principles already developed for sea clutter to the case of ground clutter, and

(2) to formulate a detailed measurement program for the collection of data on ground clutter with the radar located at the Maynard field site of the Air Force Cambridge Research Center.

The recommended measurement program required in (2) already has been submitted in a previous report [1].*

The phenomenon of radar ground clutter is a special case of wave propagation over a rough surface. In spite its being a special case, the study of radar clutter offers the possibility of throwing a great deal of light on the general problem. This is due to the fact that the accumulation of experimental data is much easier because of the coalescence of transmitting and receiving locations. By designing an experimental program to bring out certain suspected dependencies, it may be possible to arrive at the controlling physical processes in the radar clutter problem, and then to generalize from the radar to the non-radar case.

In approaching the ground clutter problem, the experience gained in the comparable study of sea clutter has been used as a guide. The sea clutter problem is somewhat less complicated because of the more restricted range of

---

* Numbers in square brackets refer to references in Sec. 9 on pp. 90-92.

irregularity of the surface. In addition, it has received much more attention in the past, out of which we have been able to deduce the presence of certain principles. Consequently, it is natural to consider the extension of these principles to the more complicated case of ground clutter.

In the sea clutter problem, the return from the sea usually represents an interference to the normal function of the radar, which is the detection and tracking of objects on or near the surface. The comparable effect also exists in ground radar operation. However, there are a number of radar applications over groun' where the ground return itself is the desired "target" information. Among these are navigation, reconnaissance, and position location by ground mapping. In these applications, the most important characteristic is the contrast between objects and their immediate surroundings, so that then interest focusses on the non-uniformity of the clutter pattern. Consequently, it is desirable to determine the factors which control the non-uniformity of the return, and, hence, the contrast in a radar map.

From the background gained in the study of sea clutter, our interest was directed toward exploring the polarization characteristics of the clutter. In the past, measurements of clutter have been made predominantly on either horizontal or vertical polarization. Some sea clutter measurements [2,3] over a wide range of angles were chiefly responsible for this deepening of interest in the polarization properties. Coupled with some concurrent theoretical results, it appeared that a more detailed study of polarization characteristics could provide valuable deductions concerning the scattering mechanism, and possibly lead to techniques by which contrast could be increased. Consequently, we have given consideration to methods by which the polarization characteristics could be measured most conveniently and accurately. As a result, we have de-

2

vised some new techniques for polarization measurements of radar character-
istics in a quantitative way. These techniques were embodied in the program
of measurements which we recommended be carried out with the Maynard field
site radar [1].

In the research carried out under this contract, we have investigated
the extension of principles which we had deduced from the sea clutter phe-
nomenon to the case of ground clutter. This includes taking into account the
absorbing characteristics of the ground, and a more general arrangement of
irregularities. We also have determined by theoretical methods the general
polarization properties of the back-scattering by small disks, including
the cross-polarized component. This represents a start toward the general
problem of the calculation of all of the properties of the return from a
ground surface.

Since the present research was an outgrowth and extension of our pre-
vious studies of the sea clutter problem, a general discussion of the latter
will provide a useful background from which to develop the extensions carried
out under the present contract. This background will be given in Sec. 2,
where the physical principles controlling the phenomenon will be brought out.
In addition, the sea clutter results referred to above, which directed espe-
cial interest to a fuller consideration of the polarization properties, will
be discussed.

In Sec. 3 the applications to the ground clutter problem of the physi-
cal principles brought out in Sec. 2 will be discussed, and experimental re-
sults will be cited for comparison.

In Sec. 4 the polarization properties of radar targets will be discussed,
the radar polarization matrix will be derived for arbitrarily oriented small

disks, and the results of some numerical calculations will be shown. The implications of the results to the interpretation of the measurements referred to earlier [2,3] then will be discussed.

In Sec. 5, radar systems which are capable of measuring the polarization matrix accurately and conveniently will be described. In particular, a new calibration technique to reduce such measurements to a quantitative basis will be shown.

In Sec. 6, extensions of our earlier scattering theory will be made to include a general arrangement of irregularities. Finally, a summary of the results obtained under the present contract will be given in Sec. 7, and recommendations for future research will be presented in Sec. 8.

4

In this section, we shall give first a general summary of the principal sea clutter properties that have been observed, and attempts at their explanation. This will be followed by a discussion of the interference phenomena between incident and reflected components as a function of the wave polarization, especially very close to a reflecting surface. The experimental tests which showed the existence of such interference effects in sea clutter will then be described. The implications of this result with respect to the fundamental scattering mechanism, which lead to the conclusion that small flat patches or facets of the surface are the principal back-scattering elements at small depression angles, then will be discussed. These mechanisms are likely to be present in the comparable ground clutter situation.

In addition, some rather recent information on polarization characteristics will be shown which are not readily explainable in terms of available polarizations characteristics. Data of this type led us to examine in detail the polarization characteristics of the return, which will be carried out in Sec. 4.

The sea clutter phenomenon is complicated by its dependence on a number of parameters, principally the depression angle (angle below the horizontal at which the sea is viewed), the polarization, the frequency, and the condition of the sea surface. Goldstein, who was perhaps the first to study the phenomenon systematically in a quantitative way, has given a thorough discussion of the results of these investigations [4]. In order to describe the back-scattering properties of the surface quantitatively, Goldstein [5] introduced a dimensionless quantity σ°, the back-scattering cross section per unit area of the sea. From measurements of this quantity, he found the

following characteristics:

(1) There is a "critical angle" below which σ^o decreases rapidly with decreasing angle, and above which it rises much more slowly, or remains constant. Furthermore, the critical angle decreases with increasing frequency.

(2) There is a pronounced polarization dependence of σ^o, which, in turn, depends on the roughness of the sea. In calm seas, horizontal polarization gives much less clutter than vertical polarization, but the difference between the two polarizations substantially disappears in rough seas, or may even reverse somewhat.

(3) The frequency dependence of σ^o varies between about λ^{-4} in calm seas to about λ^o in rough seas.

(4) At times, the area-extensive characteristic of sea clutter breaks down. On a radar with a pulse short enough to resolve individual waves, the scattering appears to be concentrated in the vicinity of the wave tops. This gives an A-scope presentation of the clutter a "spiky" appearance.

Goldstein was unable to find a satisfactory theory to explain all the above characteristics. The polarization dependence could be explained very well by a surface reflection phenomenon, which led to the supposition that water droplets thrown up from the surface were the basic scattering elements. However, this led to violent disagreement with the frequency dependence.

Katzin [6] showed that a reflection interference phenomenon, such as had been found to be important in the case of surface targets, also is important in the sea clutter phenomenon. This reflection phenomenon explains the critical angle, the polarization dependence, and the change in frequency dependence with sea roughness. It also explains the "spiky" appear-

6

ance of clutter on an A -scope at very small depression angles.

From the existence of the reflection phenomenon and the observed fre-
quency dependence, Katzin suggested the basic scattering as being due to the
small facets which overlie the main large-scale wave pattern, or swell. He
developed the theory of this mechanism and found that the facets which back
scatter most effectively at small depression angles are those whose dimen-
sions are of the order of the wavelength. He also deduced that the frequency
dependence of σ^o at small depression angles is determined by the size dis-
tribution of the facets. Furthermore, if the size and slope distributions
of the facets are independent, then, below a high-frequency limit, σ^o
should have essentially the same frequency dependence at low and high angles.
The high-angle variation was found to be determined mainly by the slope dis-
tribution of the facets. Making use of slope distributions determined from
optical measurements, σ^o was found to be approximately proportional to wind
speed at small depression angles, bur inversely proportional to wind
speed at vertical incidence. From measured values of σ^o, it appeared that
the facet mechanism could account for scattering by the entire surface of the
sea.

A discussion of the physical principles underlying these results should
be instructive, since these principles probably apply in the ground clutter
problem as well, at least in certain situations. The separate phenomena
involved are (1) interference between direct and surface-reflected waves
which affects the illumination of the scattering elements, (2) the scattering
properties of flat disks as a function of angle. In each of these, the polar-
ization of the illumination affects the type of result obtained.

7

2.1 Reflection Interference Phenomenon.

The reflection coefficient of a plane wave at a plane boundary depends on the elevation angle and polarization of the wave, and on the electrical properties of the medium below the boundary. The reflection coefficient for an arbitrarily polarized wave can be deduced from the properties for the two cases of vertical polarization (magnetic vector parallel to the boundary) and horizontal polarization (electric vector parallel to the boundary). For these two cases, the reflection coefficients are given by the well-known Fresnel relations

$$\rho_V = \frac{\epsilon' \sin\theta - (\epsilon' - \cos^2\theta)^{1/2}}{\epsilon' \sin\theta + (\epsilon' - \cos^2\theta)^{1/2}} = R_V e^{j\psi_V} \qquad (2.1)$$

$$\rho_H = \frac{\sin\theta - (\epsilon' - \cos^2\theta)^{1/2}}{\sin\theta + (\epsilon' - \cos^2\theta)^{1/2}} = R_H e^{j\psi_H} \qquad (2.2)$$

in which

θ = elevation angle of incident wave at boundary

ϵ = complex dielectric constant of the second medium

$\quad = \epsilon_1 - j\epsilon_2$

ϵ_1 = specific electric inductive capacity

$\epsilon_2 = \dfrac{\sigma}{\omega\epsilon_o}$

σ = conductivity

ϵ_o = dielectric constant of free space.

The combination of the direct and reflected waves in the space above the boundary gives rise to an interference pattern. In the case of vertical polarization, where the magnetic field is wholly parallel to the boundary, the interference pattern for the magnetic field is given by the factor

$$F_V = 1 + \rho_V\, e^{-j 4\pi \frac{H}{\lambda} \sin\theta} = 1 + R_V e^{j(4\pi \frac{H}{\lambda} \sin\theta - \psi)} \qquad (2.3)$$

where H is the [obscured] with fixed θ a[obscured] height above the boundary. From this it can be seen that, field strength [obscured] and continuous increase of height H, the resultant magnetic phase la[obscured] [obscured] will pass through alternate maximums and minimums when the π [obscured] of the reflected wave is an even or odd multiple, respectively, of [obscured] The height interval between an adjacent maximum and minimum is

$$\Delta H = \frac{\lambda}{4 \sin \theta} \qquad (2.4)$$

The electric vector, in the case of vertical polarization, has components both parallel and normal to the boundary. The normal (vertical) component has the same interference pattern as that of the magnetic vector, given above. The parallel (horizontal, or <u>longitudinal</u>) component, on the other hand, has for its interference pattern the factor

$$1 - \rho_V e^{-i 4\pi \frac{H}{\lambda} \sin \theta} = 1 + R_V e^{-i \left[4\pi \frac{H}{\lambda} \sin \theta - (\gamma_V + \pi) \right]} \qquad (2.5)$$

Thus maximums and minimums of this pattern, for fixed θ, will occur at the heights of minimums and maximums, respectively, of the magnetic field pattern given by (2.3). Consequently the resultant electric vector will be elliptically polarized, in general, for an incident vertically polarized wave. The plane of the polarization ellipse, furthermore, lies <u>in the plane of incidence</u>.

For a horizontally-polarized incident wave, the roles of the electric and magnetic vectors are interchanged. The electric vector then is parallel to the boundary, so that its interference pattern is given by the factor

$$F_H = 1 + \rho_H e^{-i 4\pi \frac{H}{\lambda} \sin \theta} = 1 + R_H e^{-i \left(4\pi \frac{H}{\lambda} \sin \theta - \gamma_H \right)} \qquad (2.6)$$

This interference pattern is same as that of (2.3) above, except that R_H and γ_H replace R_V and γ_V. Because of the difference between γ_H and γ_V, the location of a given maximum or minimum is different for the two

9

polarizations.

The resultant magnetic vector for an incident horizontally-polarized wave will be elliptically polarized in the plane of incidence. This behavior is analogous to that of the resultant electric vector in the case of an incident vertically-polarized wave, as discussed above and formulated in (2.5).

The succession of maximums and minimums of the resultant field described above gives rise to the familiar lobe structure in the coverage of a radar. We are especially interested here in the behavior below the first lobe, or first maximum. In this case the angle θ will be small in practice, so that an expansion of F to the first power in $\sin \theta$ may be used. The reflection coefficients (2.1) and (2.2) then may be written as

$$\rho_V \approx -1 + 2\epsilon'(\epsilon'-1)^{-1/2} \sin \theta, \tag{2.1a}$$

$$\rho_H \approx -1 + 2(\epsilon'-1)^{-1/2} \sin \theta, \tag{2.2a}$$

providing the second terms on the right are small compared to unity. Similarly, the exponential phase factor may be approximated as

$$e^{-j4\pi \frac{H}{\lambda} \sin \theta} \approx 1 - j4\pi \frac{H}{\lambda} \sin \theta,$$

providing the exponent is small compared to unity. Then we obtain

$$F_V \approx 2\left[\epsilon'(\epsilon'-1)^{-1/2} + j4\pi \frac{H}{\lambda}\right] \sin \theta, \tag{2.7}$$

$$F_H \approx 2\left[(\epsilon'-1)^{-1/2} + j4\pi \frac{H}{\lambda}\right] \sin \theta. \tag{2.8}$$

Thus, for sufficiently small θ, both F_V and F_H are proportional to $\sin \theta$.

The transition to (2.7) in the case of vertical polarization, and to (2.8) in the case of horizontal polarization, does not take place at the same value of θ. If the criterion for the validity of (2.1a) or (2.2a) is that the absolute value of the second term be equal to a (where $a \ll 1$), then the corresponding values of θ, denoted by θ_V and θ_H, respectively, are

10

$$\sin \theta_V = \frac{a}{2}|(\epsilon'-1)^{1/2}/\epsilon'|$$

$$\sin \theta_H = \frac{a}{2}|\epsilon'-1|^{1/2}$$

Thus

$$\sin \theta_H = |\epsilon'| \sin \theta_V \qquad (2.9)$$

For sea water in the microwave region, $|\epsilon'| \approx 70$. Consequently the transition to (2.7), for vertical polarization, takes place at a much smaller elevation angle than the transition to (2.8), for horizontal polarization. This fact is important in determining the polarization characteristics of sea clutter, for example.

Very close to the surface, where the term $a' 4\pi \frac{H}{\lambda}$ is small in magnitude compared with the other term in the brackets in (2.8), (2.7) and (2.8) become, respectively,

$$F_V \approx 2\epsilon'(\epsilon'-1)^{-1/2} \sin \theta \qquad (2.10)$$

$$F_H \approx 2(\epsilon'-1)^{-1/2} \sin \theta \qquad (2.11)$$

so that

$$F_V/F_H \approx \epsilon'. \qquad (2.12)$$

Thus, for sufficiently small angles and heights, the resultant transverse electric field strength is larger for an incident vertically-polarized wave than for an incident horizontally-polarized wave. Furthermore, the transition from (2.7) to (2.10) should take place at a higher height than the transition from (2.8) to (2.11). In fact, the transition heights should be roughly in the ratio $|\epsilon'|$. Actually the shape of the curve of F versus H is different for the two polarizations because ϵ' is a complex quantity.

On the other hand, for heights such that the term $a' 4\pi \frac{H}{\lambda}$ is much larger than the first term in the brackets in (2.7) (and therefore also in (2.8)), (2.7) and (2.8) reduce to the common relation

11

$$F \approx j\, 8\pi\, \frac{H}{\lambda} \sin\theta \qquad\qquad (2.13)$$

so that then

$$F_v / F_H \approx 1 \qquad\qquad (2.14)$$

It should be recalled that all the above relations were derived on the assumption that $4\pi \frac{H}{\lambda} \sin\theta$ is small compared to unity.

It may be helpful to consider the magnitudes of relevant quantities in the microwave region. Then $|\epsilon'(\epsilon'-1)^{-1/2}|$ is around 8, and $|\epsilon'-1|^{-1/2}$ is around 1/8. Hence in (2.7) the second and first terms in brackets have about the same magnitude when $\frac{H}{\lambda} \approx 0.6$, while in (2.8) this equality takes place at $\frac{H}{\lambda} \approx 0.01$. Consequently, F will be given by (2.13) for almost all cases for horizontal polarization, and also for vertical polarization for values of $\frac{H}{\lambda}$ greater than about 3.

The implications of the above properties to the clutter problem will be discussed below.

2.2   Experimental Test of Reflection Interference

As a preliminary to discussing the application to sea clutter of the reflection interference phenomena discussed above, we shall consider the behavior of a radar target which extends up from the surface to a height H, say. If this height is large relative to $\lambda/(4 \quad$ (see (2.4)), then the target will cover more than one lobe of the interference pattern, so that the target will effectively integrate out the field variation over the lobes. This actually produces a net increase of gain over the incident field acting alone, the gain being due to the field reflected by the surface. As the range of the target is varied (with fixed antenna and target heights), the depression angle θ will vary, so that the lobe structure will shift along

12

the target. Due to the integrating effect just mention d, however, the average ratio of back-scattered to incident field will remain substantially the same. Thus, the variation of received echo power with range will be the same as in free space, i.e.,

$$P_R \propto R^{-4},$$

where R is the range.

However, if the top of the target lies below the first lobe of the interference pattern, then the resultant field at the target will decrease monotonically from the top to the surface. This is the region where the interference pattern is given by (2.7) and (2.8), in which the factors F_v and F_μ are proportional to $\sin \theta$. Since the depression angle of the image of the top of the target is given by

$$\sin \theta = \frac{H_i + H}{R}, \qquad \qquad (2.15)$$

where H_i is the height of the radar, an increase of R will result in a decrease of $\sin \theta$, and hence a corresponding decrease of F. Since these factors apply to the resultant incident field strength at the target, the echo field strength involves F^2, so that the received power density is proportional to F^4. Thus, in this region of depression angle

$$P_R \propto R^{-4} F^4 \propto R^{-8}. \qquad \qquad (2.16)$$

Fig. 2-1 shows the results that would be expected on the basis of the reflection interference phenomenon for a surface target. Between the R^{-4} and R^{-8} regions, which may be called the near and far zones, respectively, a smooth transition occurs. If the transition range, R_t, is defined as the intersection of the R^{-4} and R^{-8} lines, then it is found that for a surface target of uniform cross section over a plane surface of reflection
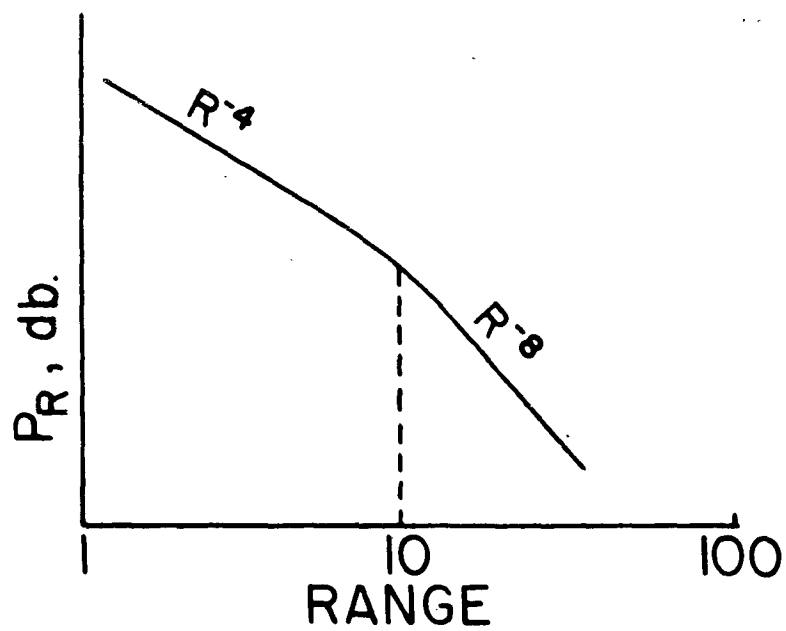
FIG. 2-1

Theoretical form of received power vs. range
for a surface target

14

coefficient -1, with a radar height H_1,

$$R_t = \frac{H_1 H}{0.195 \lambda} \qquad (2.17)$$

For a given target, then, the transition range will be directly proportional to frequency and to the radar height H_1.

Fig. 2-2 shows experimental results obtained on a surface vessel as radar target. The good agreement between the theoretically predicted type of variation in Fig. 2-1 is evident. The more rapid decrease with range of the points at the extreme right of the plot in Fig. 2-2 is due to the earth's curvature, which was neglected in the calculations for Fig. 1.

If the target is very wide, so that it completely fills the radar beam in its azimuthal extent, then the effective width of the target is $R \Phi$, where Φ is the azimuthal beamwidth. This is the case when the "target" is the sea surface. Hence, instead of R^{-4} and R^{-6} dependencies in the two regions discussed above, R^{-3} and R^{-7} dependencies, respectively, would be obtained.

Precisely this type of behavior was found in some early sea clutter measurements on airborne radar, using horizontal polarization. Fig. 2-3 shows an example of this. This type of result, therefore, is strongly suggestive of a reflection interference mechanism operating in the sea clutter phenomenon.

In order to submit this suggestion to a critical test quantitative measurements of received sea clutter power were made for a wide range of radar heights and frequencies. According to (2.17), if measurements are made under the same sea conditions, the values of received clutter power at various altitudes, on a given frequency, should give a family of curves such as shown in Fig. 2-4. These curves should join together smoothly into a

RECEIVED POWER vs RANGE

LST # 998   ZIG-ZAG STERN
22/2/45   2100-2250
MK-12   970 Mc/s

R^4

R^8

RANGE IN YARDS

db

70
60
50
40
30
20
10
0

1000   10,000   100,000
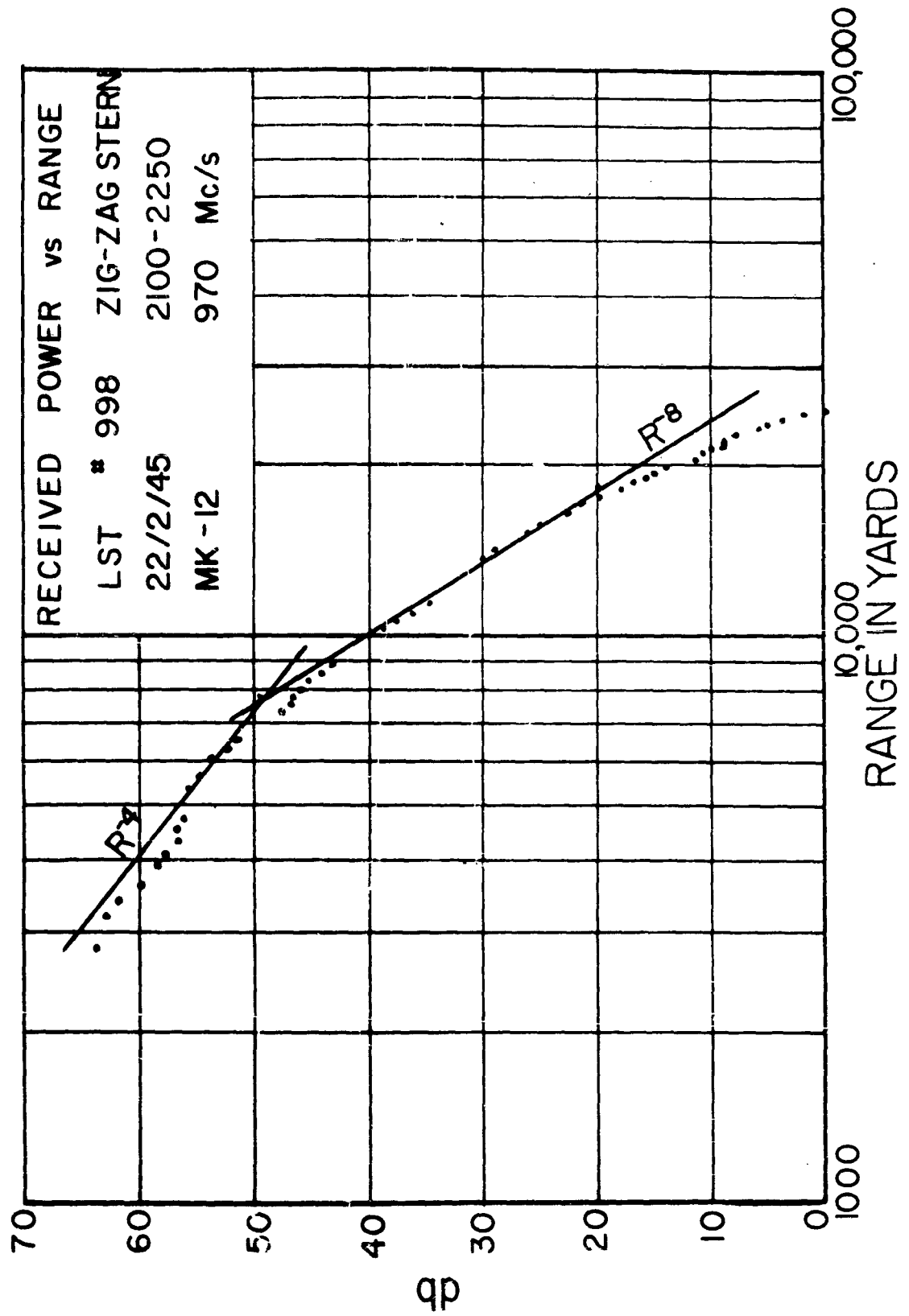
FIG. 2-2 Measured power vs. range for a surface vessel

16

Fig. 2-5 Measured sea-clutter power plotted against norm coordinates.

Fig. 2-4 Form of σ vs. R curves for various radar heights.
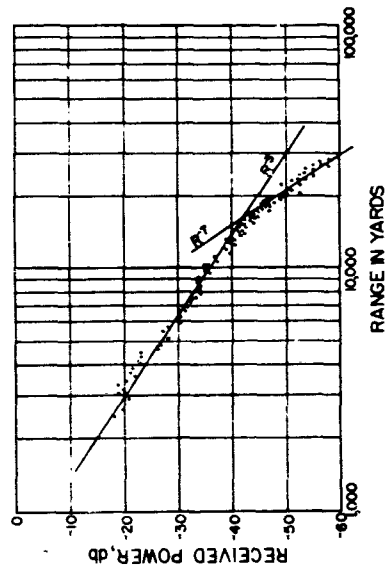
Fig. 2-3 Received sea-clutter power vs. range. $\lambda = 3.2$ cm, radar height 1000 feet.

17

single curve if the various bra- k- o; "lg. ..h -e "slid" along the R^{-3} line until their transition ranges coincide. This is attained by using as abscissa the quantity log $\left(R/R_{\chi}\right)$, and as ordinate, log $\left(\sigma R_{\chi}^{-3}\right)$. Further-more, if σ^o is independent of frequency, then the graphs on the several frequencies, after normalization to constant beamwidth, should match when superimposed; any adjustment vertically (without shift of abscissa) re-quired to produce a match is then due to the variation of σ^o with frequency.

Fig. 2-5 shows the result of such a superposition of the results for three wavelengths (3.2, 9.1, and 24 cm) and for six altitudes from 200 to 10,000 feet. This is a composite plot of 17 different runs. The agreement with the type of behavior expected on the basis of the reflection mechanism is striking, especially in view of the fact that some wind speed variations occurred during the time required to make the measurements (approximately $2\frac{1}{2}$ hours). This agreement lends strong support to the reflection mechanism.

From the measurements, one can use (2.17) to deduce the effective target height H from the observed transition ranges. When this is done, it is found that H is much less than the measured wave height. This indicates that the reflection takes place somewhere between the troughs and crests of the sea waves.

The measurements discussed above were made with horizontally polarized waves. A comparable set of measurements was not made with vertically polar-ized waves. One would expect, on the basis of the interference pattern characteristics discussed in Sec. 2.1, that the transition range for vertical polarization would be much larger than for horizontal polarization. In fact, it follows from (2.9) and (2.15) that, aside from any possible effects of the earth's curvature, the transition ranges should be in the ratio $|\epsilon'|$.

Furthermore, if the relations are such that (2.10) and (2.11) apply (i.e., the range is greater than the transition range for vertical polarization, and $4\pi \frac{H}{\lambda} << |\epsilon'-1|^{-1/2}$), then in virtue of (2.12)

$$(P_R)_V / (P_R)_H \propto |\epsilon'|^4 \frac{\sigma_V^o}{\sigma_H^o} \qquad (2.18)$$

On the other hand, if $4\pi \frac{H}{\lambda} >> |\epsilon'(\epsilon'-1)^{-1/2}|$, then, in virtue of (2.14)

$$(P_R)_V / (P_R)_H \propto \frac{\sigma_V^o}{\sigma_H^o} \qquad (2.19)$$

For the sea clutter problem, H is to be identified with the sea wave height. Consequently, the observed polarization ratio should depend on sea roughness, decreasing in rough seas. Since H appears in the ratio $\frac{H}{\lambda}$, a given sea is effectively rougher at higher frequencies.

The intermediate condition, where $|\epsilon'(\epsilon'-1)^{-1/2}| >> 4\pi \frac{H}{\lambda} >> |\epsilon'-1|^{-1/2}$ is quite likely to occur, in which case

$$(P_R)_V / (P_R)_H \propto \frac{|\epsilon'(\epsilon'-1)^{-1/2}|^4}{(4\pi \frac{H}{\lambda})^4} \cdot \frac{\sigma_V^o}{\sigma_H^o} \qquad (2.20)$$

Under these conditions the frequency dependence of the ratio $(P_R)_V / (P_R)_H$ is affected by the factor $\frac{H}{\lambda}$ in the denominator.

From the above discussion, it follows that the dependence of the apparent value of σ^o on polarization is a function of the sea roughness. The ratio of normalized clutter power with vertical polarization to that with horizontal polarization should be greater for calm seas than for rough seas, and sea roughness should affect the frequency dependence. This is precisely what Goldstein found from his measurements.

It is easy to see from (2.13) that for sufficiently small depression angles the received clutter power is proportional to H^4. Hence, isolated prominent wave crests should give much stronger echoes than the surrounding sea. Consequently, at very small depression angles the uniformly noise-like structure

19

of the sea echo should break up into discrete groups. This provides an explanation for the so-called "spiky" clutter which has been observed on pulse radars whose pulse lengths are not short enough to resolve the waves [6].

Thus it is seen that the reflection interference mechanism explains many of the perplexing properties of sea clutter; namely, the "critical angle" (which corresponds to the transition range), the polarization properties, the change in frequency dependence with sea roughness (or $\frac{H}{\lambda}$), and the spiky appearance of sea clutter on an A-scope at very small depression angles.

2.3 Fundamental Scattering Mechanism.

From the reflection mechanism discussed earlier, many of the previously reported characteristics of sea clutter have been shown to be explainable. Hereafter, it will be assumed that the effects of the reflection mechanism have been taken into account in deducing the value of σ^o from the measured value of P_R,[*] so that σ^o refers to the basic scattering properties of the surface. Then the experimental data show that σ^o is a slowly-varying function of frequency.

The plot of the measurements in Fig. 2-5 was designed to verify the suspected reflection interference phenomenon. It also has other implications. The range of depression angles spanned in the plot is from less than 1° to over 15°. Hence σ^o for horizontal polarization must be substantially constant over this range of angles.

When the measurements were evaluated in terms of the calibration constants measured for the equipment, it was found that σ^o in the above angular

---

[*] In fact, this usually is not done in presenting experimental data, so that the data usually have to be interpreted in terms of the presence of the reflection-interference mechanism.

20

range was about 10^{-4} (-40 db) or less for $\lambda = 10$ cm, depending somewhat on the roughness of the sea surface. This means that 1 square meter of sea surface scattered back 10^{-4} or less of the power incident on it. Since sea water is a good reflector, this implies that the scattering elements must be very directive, presumably scattering most strongly in the forward direction, and very little back toward the radar. Since a flat plate is the most directive surface known for plane waves, this led to the investigation of the scattering properties of an array of flat plates, or facets, as the basic scattering elements of the sea surface. The basic physical principles of the scattering process will be traced here, since these principles are likely to be important in the ground clutter problem as well.

2.3.1 Scattering By Flat Plates.

(a) Scattering at Small Depression Angles.

For a flat plate which is large relative to λ, the maximum back scattering occurs when the plate is parallel to the incident wave front, since then all elements of the plate are excited in phase and re-radiate in phase. Denoting the area of the plate by A, the gain of the plate as a re-radiator is $4\pi\frac{A}{\lambda^2}$, so that the back-scattered power is proportional to $4\pi\frac{A^2}{\lambda^2}$. To fix the discussion, assume that the plate is rectangular, lies in a vertical plane, and that the incident wave normal is horizontal (see Fig. 2-6). If the plate is then tilted about a horizontal axis perpendicular to the wave normal, say by an angle θ which is greater than the half-width of the main scattering lobe, a progressive phase lag between the farther and nearer elements of the plate will be introduced. If we divide the plate into small strips in pairs, where the two strips of

21
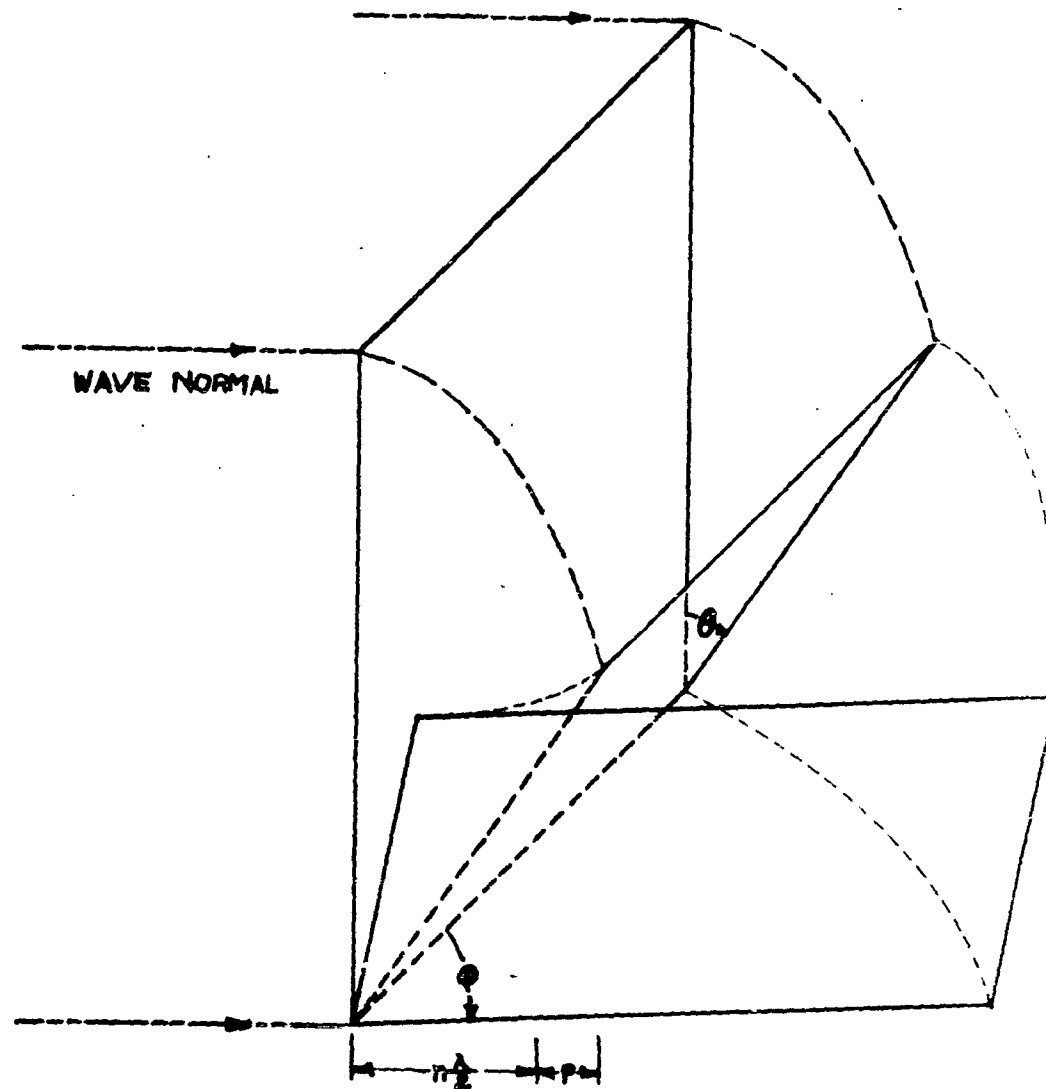
WAVE NORMAL

FIG. 2-6

Illustrating relations for flat plates at various orientations
to the wave normal

22

a pair are separated along the wave normal by $\lambda/4$, then the round-trip difference in distance will be $\lambda/2$, so that the fields from the two strips of a pair will cancel in the backward direction. Hence the part of the plate which has a projection $n\lambda/2$ along the wave normal (n an integer) will produce no field in the backward direction, since all of this part may be divided up into pairs of strips separated by $\lambda/4$. It follows that the field in the backward direction is equal to that produced by just the end piece whose projection is smaller than $\lambda/2$. Furthermore, the contribution of this piece will be maximum when its projection equals $\lambda/4$. Hence, for an inclined plate whose projection along the wave normal is greater than $\lambda/2$, the maximum back-scattered field is independent of the length of the plate. Since the total field intercepted by the plate is proportional to $\cos\theta$, it follows that for inclined plates the maximum back scattering varies as $\cos^2\theta$, and thus increases as the angle between the plane of the plate and the wave normal is increased.

Similarly, if the inclined plate is given an additional tilt at right angles to the tilt just discussed (i.e., in the φ-direction) by an amount greater than the half-width of the main lobe, so that the width elements are no longer excited in phase, the maximum back scattering then also becomes independent of the width, and hence completely independent of the size of the plate.

If we consider the application of these principles to the scattering at small depression angles by the facets of the sea surface, it becomes evident that, for those plates which are large relative to the wavelength, the important back scattering will come from the front part, or heads, of the wave crests, where the slopes are steepest and face the radar. Quantitatively,

the dependence of the back-scattering (radar) area σ on plate area A, for large plates, is as follows:

(a) normal incidence: $\qquad \sigma \propto A^2/\lambda^2, \qquad \sigma/A \propto (A/\lambda^2)$;

(b) θ-tilt: $\qquad\qquad \sigma \propto A, \qquad\qquad \sigma/A \propto (A/\lambda^2)^0$;

(c) θ-tilt and φ-tilt: $\quad \sigma \propto \lambda^2, \qquad\qquad \sigma/A \propto (A/\lambda^2)^{-1}$

For an ensemble of plates with a given θ-tilt and various φ-tilts, the average value, $\bar{\sigma}$, of σ is intermediate to (b) and (c) above, or

$$\bar{\sigma} \propto A^{1/2}, \qquad \bar{\sigma}/A \propto (A/\lambda^2)_o^{-1/2}$$

The quantity $\bar{\sigma}/A$ is the important one for assessing relative contributions to σ^o, since the number of plates of a given size which can be accommodated in a unit area of surface is inversely proportional to the plate area.

For circular s, the symmetry of the situation allows the inclination of the plate to be measured by the single angle θ between the wave normal and plate normal. Then it is found that

$$\sigma \propto \lambda A^{1/2}, \qquad \sigma/A \propto (A/\lambda^2)_o^{-1/2}$$

This is intermediate to (b) and (c) above, and is the same as the average of an ensemble of rectangular plates distributed over a range of φ-angles. From this relation it is evident that for "large" plates, the larger the plate the smaller is its average contribution to σ^o.

For plates which are small relative to λ, on the other hand, the scattering is not strongly dependent on angle, and is proportional to D^6/λ^4, so that

$$\sigma \propto A^3/\lambda^4, \qquad \sigma/A \propto (A/\lambda^2)^2$$

Thus, for "small" plates, the contribution to σ^o is larger the larger the plate.

From the relations for "large" and "small" plates given above, it is

24

apparent that there must be some intermediate range of plate size (measured in terms of λ^2) which is most effective for small-angle back scattering. Since the quantitative relations in this intermediate range are not available in easily calculable form, the "small" and "large" size relations may be extrapolated into the intermediate region until they meet to obtain an approximate behavior.

For facets which are circular disks, the resulting behavior as a function of plate size for several values of facet tilt are shown in Fig. 2-7. From this it is found that the optimum diameter, D_i, is about $\lambda/2\pi$, or the perimeter is about a half-wavelength. In effect, then, the operating frequency focuses attention on the facets whose dimensions are of the order of the wavelength ($2\pi D/\lambda \approx 1$). From this, one would expect that the frequency dependence of σ^o would be linked to the size distribution of the facets. This is borne out by a quantitative analysis.

It is instructive to make calculations for a hypothetical sea surface in which all the facets are the optimum size D_i. If N is the number of facets, of diameter D_i, per unit area of sea, and if their relative phases vary randomly, then $\sigma^o = N\sigma_i$. For $\theta = 30^o$, we find $D_i/\lambda = 0.171$, $\overline{\sigma_i} = 2.62 \cdot 10^{-3}\lambda^2$, so that $\sigma^o = 2.62 \cdot 10^{-3}N\lambda^2$. Hence to produce a value of 10^{-4} for σ^o would require $0.038/\lambda^2$ facets of optimum size per unit area of sea. Since there can be at most only about $1/D_i^2 = 34.2/\lambda^2$ facets per unit area, it is evident that the postulated mechanism requires $0.038/34.2$ or only about 10^{-3} of the maximum value for the back scattering. This allows for sizes departing considerably from the optimum value.

Actually, of course, not all of the facets are of the same size or slope, so that a distribution of sizes and slopes needs to be considered. Since, as
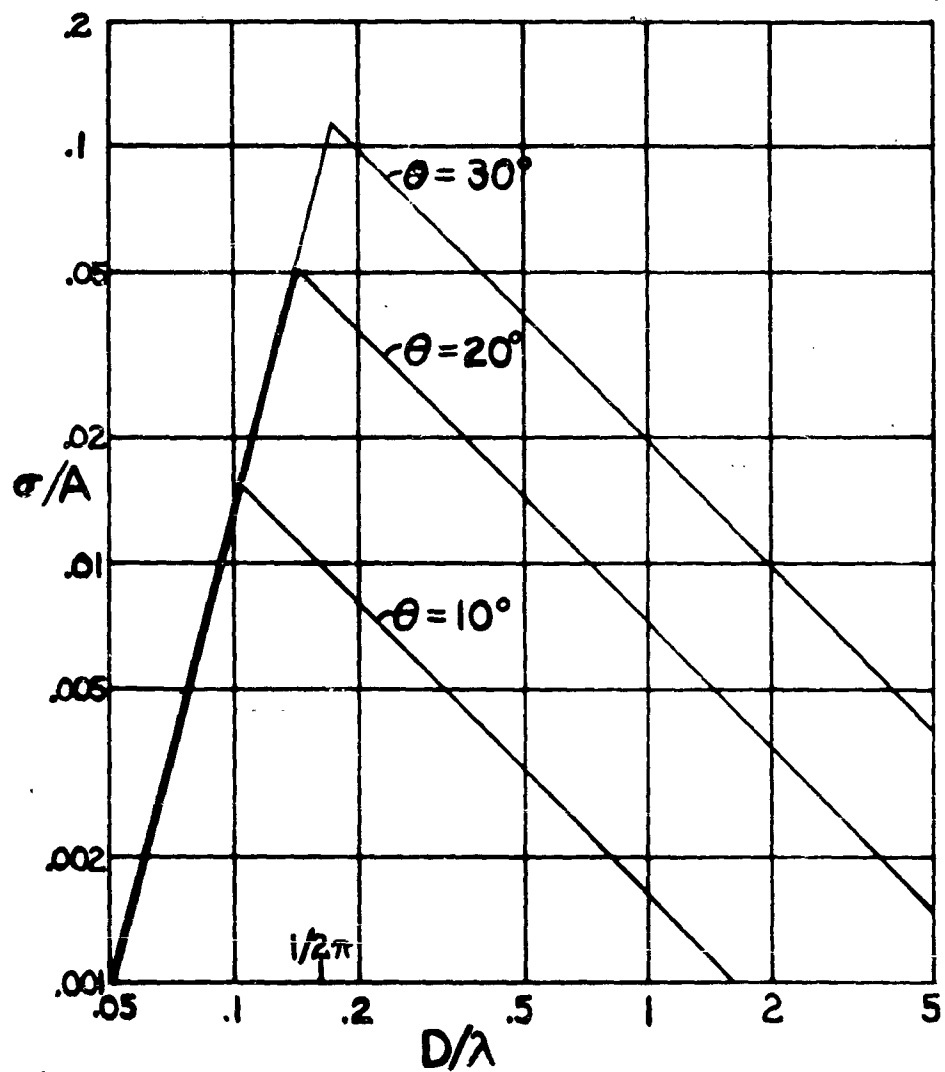
25

FIG. 2-7

σ/A for inclined circular disks.

26

pointed out above, the operating frequency enhances the facets whose perimeter is about a half-wavelength, it is readily seen that the functional form of the size distribution determines the frequency dependence of σ^o, and vice versa. If, for example, $\sigma^o \propto \lambda^{-1}$, then the average number, N, of facets of area A, per unit area of sea surface, is found to be given by $N \propto A^{-5/2}$. In general, if

$$\sigma^o \propto \lambda^{-n},$$

then

$$N \propto A^{-\left(2 + \frac{n}{2}\right)}.$$

(b) Scattering at Large Depression Angles.

The facet mechanism allows the qualitative and quantitative variation of σ^o at large angles to be deduced quite readily [6,7]. At high angles some of the facets are viewed broadside, so that these give a preponderant echo, which will be proportionately stronger the larger the facet. The back-scattering area of a large flat plate at normal incidence is $4\pi A^2/\lambda^2$, where A is the area of the plate. Of this, A represents the power intercepted by the facet, and $4\pi A/\lambda$ its gain. This indicates that large plates are proportionately more important back scatterers at normal incidence. However, the solid angle of the back-scattering pattern is proportional to λ^2/A. Hence, for a distribution of facet slopes the overlapping of the patterns of facets having slopes differing by a given amount will be less the larger the facet. For a bivariate slope distribution, the extra gain of a large facet thus is just counter-balanced by the reduction in overlapping of facet patterns, due to the narrower pattern width, so that the total back-scattered power in the main lobe of the pattern is about equal to the power intercepted

by the facet. The variation of σ^{-o} with angle then will be similar to the slope distribution, and will differ from the slope distribution only by the broadening due to facets of intermediate size (measured in units of λ) which have relatively wide patterns. Consequently, information on slope distribution should provide a means of determining σ^o for large depression angles, especially near vertical incidence.

Measurements of slope distribution of the facets of the sea surface have been made by optical methods. These show that the distribution is approximately Gaussian, but is more peaked, and is skewed in the upwind-downwind direction. Fig. 2-8 shows the upwind-downwind distribution, and Fig. 2-9 the crosswind distribution, for wind speeds of 10 and 20 knots. The ordinate in these figures is the probability density of facet slope. It is interesting to note that the distribution curve becomes broader and of lower peak amplitude as the wind speed increases. Since, as pointed out above, the variation of σ^o with angle is similar to the slope distribution, these curves also indicate the general way in which σ^o varies in the neighborhood of vertical incidence. Therefore, higher wind speeds result in smaller values of σ^o at vertical incidence and a flatter angular variation.

The theory of back scattering by facets outlined above thus yields the following characteristics: The facets which back-scatter most effectively at small depression angles are those whose perimeter is about a half-wavelength. The frequency dependence of σ^o is linked with the size distribution of the facets. The variation of σ^o in the neighborhood of vertical incidence is determined mainly by the slope distribution of the facets, becoming flatter with increasing wind speed. At small depression angles σ^o increases with wind speed, while at vertical incidence it decreases with wind speed.
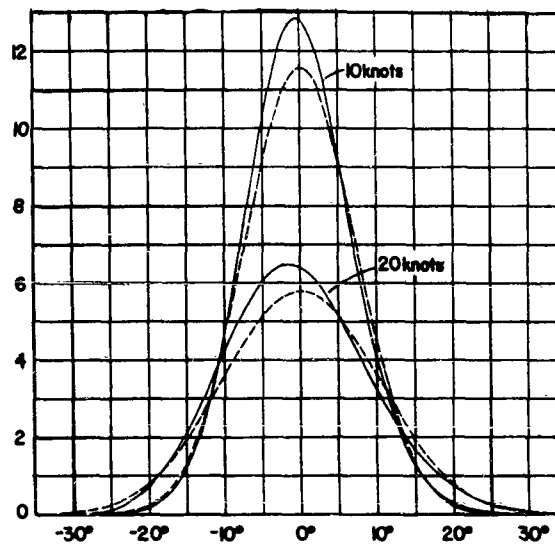
Fig. 2-8   Upwind-downwind facet slope
           distributions as determined
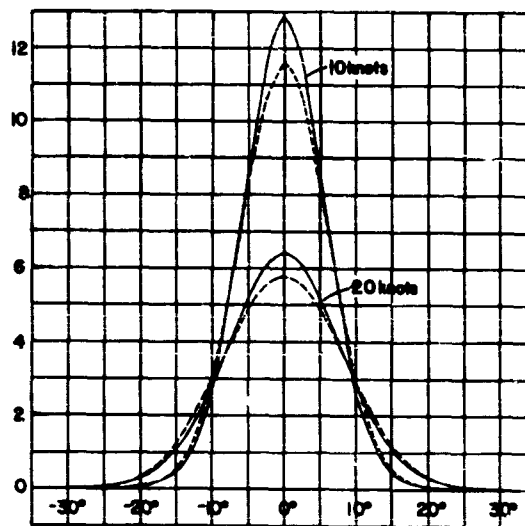   by optical measurements.

Fig. 2-9   Crosswind facet slope distri-
           butions as determined by
           optical measurements.

29

These characteristics agree quite well with the rather limited measurements which have been made over a wide range of depression angles. This agreement lends encouragement to an application of the same physical principles to the ground clutter problem. This will be taken up in Sec. 3 of this report.

2.4 Recent Polarization Data.

In a recent preliminary report [2], Spetner and Katz drew attention to two sets of data which seemed to them to refute the reflection interference explanation of the polarization dependence of sea clutter at small depression angles. The results they cite are reproduced here as Figs. 2-10 and 2-11. Fig. 2-10 shows results obtained by M. H. Oliver and his associates at R.R.E. in England. This is part of a very careful set of measurements that is considered to be very reliable. For depression angles in the range 0.6° to 2.4° this figure shows that vertical polarization gives 3-5 db _less_ return than does horizontal polarization. It should be noted that these results were obtained in sea state 1. Fig. 2-11, on the other hand, shows the results of measurements by NRL which were obtained in a 30-knot wind. The curve as drawn for vertical polarization shows a tendency to drop very rapidly at the small-angle end, thus suggesting that a crossover will take place at some smaller depression angle. On the other hand, Fig. 2-12 shows the original NRL [3] plot from which Fig. 2-11 presumably was derived. This plot exhibits no tendency for the vertical polarization curve (labeled VV) to overtake the horizontal curve (labeled HH). However, this figure is noteworthy in that it gives the first published data on cross polarization measurements. It is striking that the general level of the cross polarized return is about equal to that of the horizontally

30

RADAR CROSS SECT·
SEA RETURN
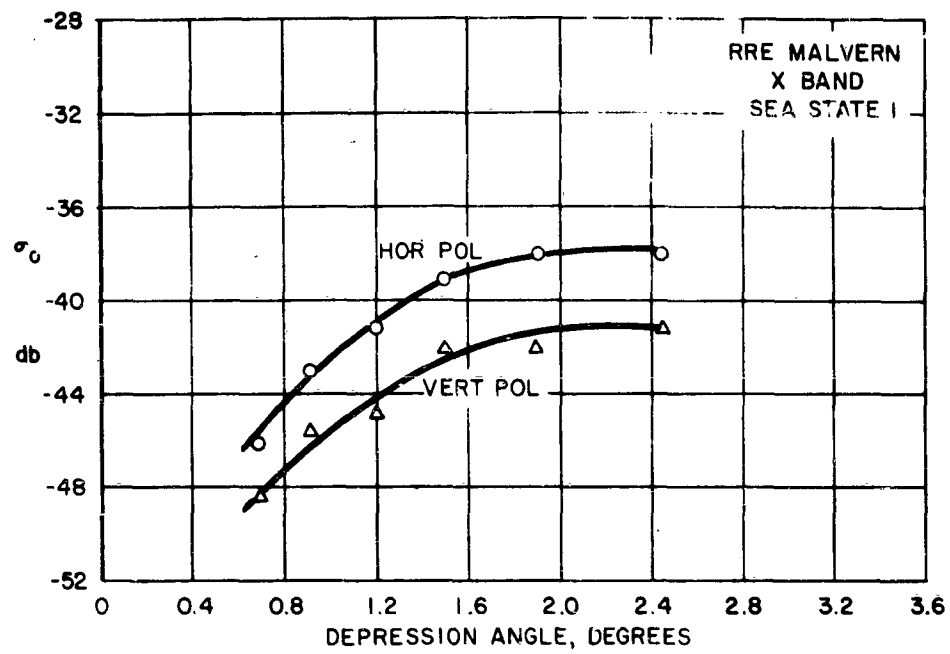

FIG. 2-10   RRE Sea clutter measurements for horizontal and vertical polarizations
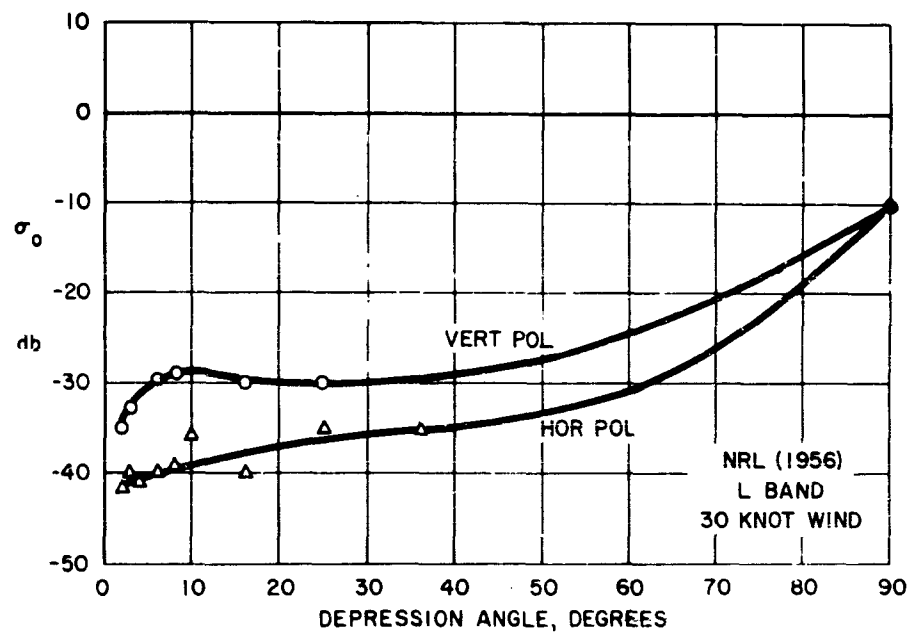
RADAR CROSS SECTION
SEA RETURN

FIG. 2-11   NRL Sea clutter measurements for horizontal and vertical polarizations

31
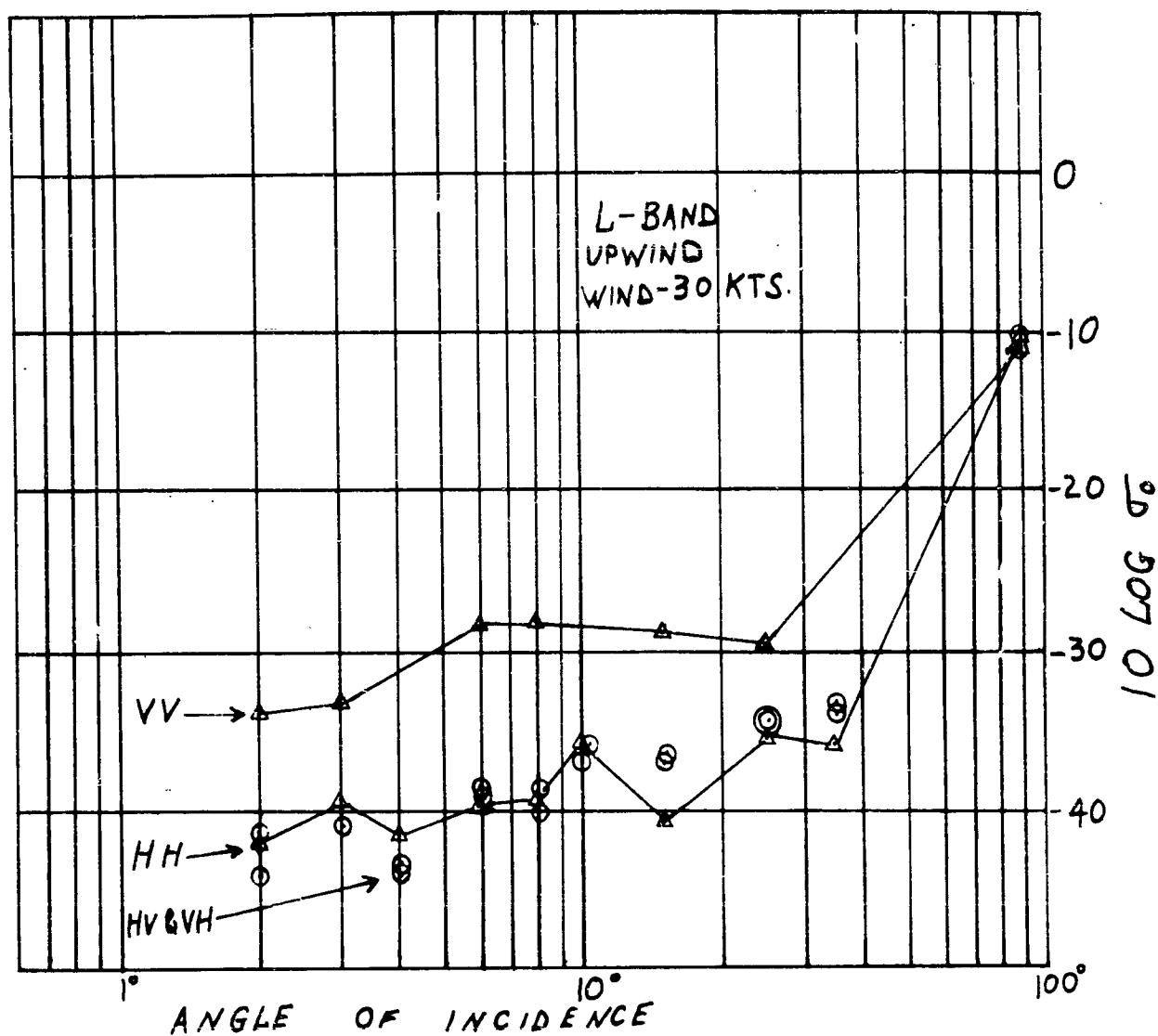
FIG. 2-12

NRL Sea clutter measurements for various polarizations.
HH = Horiz. pol. transmitted, Horiz. pol. received;
HV = Horiz. pol. transmitted, Vert. pol. received;
etc.

32

polarized return.

Thus there are two features of the polarization dependence exhibited in these figures which are noteworthy. Fig. 2-10 shows unambiguously that, under certain conditions, vertical polarization can give less return at very small depression angles than horizontal polarization. Fig. 2-12 poses the question as to how such a large cross polarized component is generated.

As a result of these characteristics, our interest was directed to a fundamental consideration of the polarization characteristics of ground and sea clutter. Our theoretical results are given in Sec. 4. From these results, it is possible to arrive at a satisfactory explanation of the polarization characteristics shown in Figs. 2-10 and 2-12.

3. APPLICATIONS TO GROUND CLUTTER CHARACTERISTICS.

3.1 Physical Processes.

In the preceding section, it was shown that a study of sea clutter characteristics led to the recognition of the existence of the following physical processes:

(a) reflection interference which controls the illumination of the scattering elements; this is a function of the height distribution of the surface irregularities (measured in wavelength units) above the mean surface level;

(b) the off-angle scattering characteristics of flat elements of the surface, which result in the relationship of the frequency dependence of σ^c to the size distribution of the elements;

(c) the near-broadside characteristics of such flat elements, which relates the high-angle variation of the scattering to the slope distribution of the elements.

In this section, the application of the above physical processes, and others, to the ground clutter phenomenon will be considered.

In the sea clutter problem, the reflection coefficient of a plane element of the sea is sufficiently high that it may be considered to be unity in the neighborhood of normal incidence for any linear polarization. For ground clutter, however, it should be expected that the reflection coefficient usually would be significantly less than unity. Since the dielectric constant and conductivity of the soil, which determine the reflection coefficient, vary considerably with type of soil and with moisture content, the effects of these factors need to be taken into account.

34

In the sea clutter problem, the variation of σ^o with angle and with frequency could be deduced in terms of the slope and size distributions of flat elements, or facets, of the sea surface. The types of irregularities which may characterize the surface of a body of water are limited by the distorting forces of the wind and the restoring forces of gravity and surface tension. In contrast, the irregularities of the surface of the ground may take myriad forms. Consequently it is not safe to assume a single form of surface element as the typical elemental scatterer to explain ground clutter characteristics. Rather, typical elemental surface forms probably should be divided into classes, and the scattering characteristics of each class determined. In particular, many forms of vegetation and culture have a pronounced preference for vertical or near-vertical elements.

From the above discussion, it is evident that a treatment of the general ground clutter problem requires the consideration of other physical processes than those given in (a) — (c) above. These include:

(d) the reflection coefficient of the scattering elements;

(e) the types and scattering characteristics of various typical classes of ground irregularities.

In this section we shall discuss some of the available data on ground clutter to point out instances in which some of these principles make themselves evident.

3.2 Interpretation of Clutter Measurements.

The interpretation of clutter measurements in order to arrive at the physical characteristics of the scattering phenomena involved merits some general comment before the results of measurements are portrayed for discussion.

35

Clutter measurements have been made both with ground-based radars and with airborne radars. In the former case, the clutter pattern is more or less fixed, except for some internal motion of the scattering elements caused by wind, or due to moving elements such as vehicles. Airborne radars, on the other hand, move over the terrain with a relatively high velocity, so that they usually scan a changing area and thus determine some average over the variations which occur from point to point. Depending on the homogeneity of the terrain, therefore, the type of angular dependence obtained from the two types of measurement may not be the same. In particular, a $\sigma^{\bullet}$ versus angle plot is likely to be much smoother for airborne measurements than for ground-based measurements.

Another point which must be kept in mind is that a plot of σ^{o} versus angle is deduced from measurements with a radar system which has an elevation pattern of finite width. If the portion of ground which contributes to the scatter measurement is limited by the elevation angle beamwidth of the antenna, and if the scattering varies appreciably over the angular range of the antenna pattern, the deduced angular variation will be less than the actual variation. This is the typical case of antenna smoothing of distributed sources. A particular instance of this smoothing occurs near vertical incidence in the case of sea clutter. For very low wind speeds and a calm sea, σ^{o} varies greatly in an angular range of a few degrees. Under such conditions, the measured angular variation is not as rapid as the true variation because of the finite antenna beamwidth.

A final comment regarding the interpretation of measured data in terms of physical processes or models is deemed worth of mention at this point. In only relatively few cases is the measurement of the angular dependence made

36

over substantially the entire angular range $0^{\circ}-90^{\circ}$. Thus often a range of $10^{\circ}-20^{\circ}$ at one or both ends of this range is not included in the measurements. With such limited data it usually is not possible to make reliable deductions concerning the mechanisms involved, or to decide between competing processes or models. This will be brought out clearly in certain cases to be discussed below.

3.3 Selected Data on Ground Return.

In this section we shall show some data on ground return selected from unclassified sources. These will be discussed in the light of the possible physical processes mentioned in Sec. 3.1. In each case, the data are stated to represent absolute values of σ^{o}, rather than relative values. Data have been selected for various frequencies, for both horizontal and vertical polarization, and for a   of terrains. Both airborne and ground-based data are included, so that the effects of terrain inhomogeneity are made evident.

In making the selection of data for discussion, we have avoided two extreme classifications. These are (1) cities, and (2) unusually flat surfaces such as paved roadways and closely cropped vegetation. Thus the data presented refer to the wide range of terrain encompassed in the very loose and ill-defined term "average terrain".

3.3.1 Ground-based Measurements.

Figs. 3-1 — 3-3 show measurements made by Grant and Yaplee [8] at three frequencies over three samples of terrain. Vertical polarization was used. The three frequencies were 9.3, 24, and 35 kmc (λ = 3.2, 1.25, and 0.86 cm). The equipment in each case was set up at a fixed location at a

37

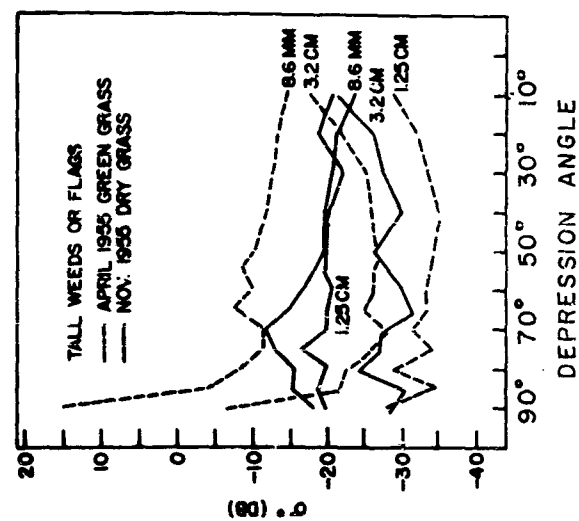Fig. 3-3 σ^{o} for a nonhomogeneous terrain.

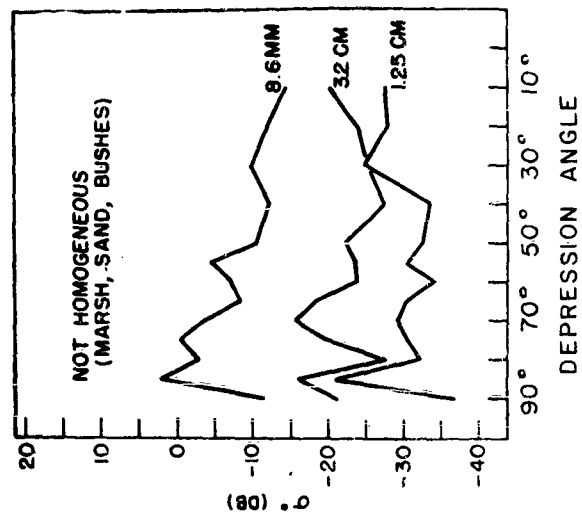Fig. 3-2 σ^{o} for a tree-covered terrain.

Fig. 3-1 Comparison of σ^{o} for dry and green grass.

38

height of 100-150 feet above the ground, and readings taken at $5°-10°$ steps in elevation angle. In all three cases shown, the effects of terrain inhomogeneity are apparent, to varying degrees.

Fig. 3-1 shows $\sigma^°$ versus angle for a flat terrain covered with grass and tall weeds. The solid lines represent measurements made in November when the ground was dry, while the dotted lines show measurements made in April when the ground was wet and the vegetation was green. Several interesting features in these results are worth pointing out. These can be broken down as follows:

(a) Ground Dry

(1) Angular dependence: Aside from the irregular course of the curves (presumably due to terrain inhomogeneity), there is no uniform feature of the variation with angle. At 3.2 cm there is a distinct upward progression from $40°$ to $10°$. At 1.25 cm there is no significant trend with angle over the entire range. At 8.6 mm there is a distinct hump around $70°$ and a droop in level at small angles.

(2) Frequency dependence: There is a general increase in signal level with frequency, although the amount of the increase is not uniform for all angles (since the angular dependence is not the same at the three frequencies).

(3) Average levels:

(cm):	3.2	1.25	0.86
(db):	-27	-20	-18

(b) Ground Wet

(1) Angular dependence: A striking feature is the sharp rise to a prominent peak at vertical incidence on both 3.2 and 0.86 cm. The upward-progression from $40°$ to $10°$ now is evident both at 1.25 and 3.2 cm. The

39

0.86 cm variation, aside from the peak at vertical incidence, is about the same as before.

(2) Frequency dependence: There is still an increase in signal level from 3.2 to 0.86 cm., but the 1.25 cm level has shifted downward to considerably below that at 3.2 cm.

(3) Average levels: Disregarding the peak at vertical incidence, the values are

λ (cm):	3.2	1.25	0.86
σ°(db):	-24	-32	-12

Aside from an anomaly at 1.25 cm (suspected to be due to the water vapor absorption line at this wavelength), the ground when wet gives from 3 to 6 db higher return than when dry. A natural presumption is that this is due to the increase in reflection coefficient due to the water. The sharp peak at vertical incidence is suggestive of specular reflection associated with flat areas ("optically flat" in terms of the wavelength of measurement) of appreciable size. These can be considered as facets such as proposed in sea clutter theory [6,7]. The sharpness of the peak indicates that the slopes of such flat areas are distributed over a very small range of angles. In fact, the measured sharpness probably is determined by the finite antenna beamwidth (approximately 3° in each case).

Fig. 3-2 shows measurements for a terrain covered by trees in full foliage. The characteristics may be summarized as follows:

(1) Angular dependence: No significant variation.

(2) Frequency dependence: A general increase of σ° with frequency is evident.

(3) Average levels:

40

λ (cm):	3.2	1.25	0.86
σ° (db):	-27	-18	-15

Fig. 3-3 shows the results for a terrain, characterized as "not homogeneous", consisting of marsh, sand, and bushes. The general features are

(1) Angular dependence: Very irregular, with general downward trends at the two shorter wavelengths. (The reduction at vertical incidence is stated as being due to debris.)

(2) Frequency dependence: An increase from 3.2 to 0.86 cm, with an inversion (decrease) at 1.25 cm. This is similar to the anomaly noted in connection with Fig. 3-1 when the ground was wet.

(3) Average levels:

λ (cm):	3.2	1.25	0.86
σ° (db):	-23	-28	-8

3.3.2 Airborne Measurements.

Figs. 3-4 — 3-6 are composite plots of an extensive series of airborne measurements made by the Goodyear Aircraft Corporation [9]. Eleven different terrain samples are shown, taken in various parts of the country. All of these measurements were made at 9.4 kmc, with horizontal polarization. In Figs. 3-4 and 3-5 the depression angle range represented is 10°-65°, or less, while in Fig. 3-6 the lower angular range has been pushed down to less than 1°.

Fig. 3-4 contains four samples of return from vegetation, ranging from a rolling meadow to forests. All four samples have the same general character and remarkably similar range of variation with angle. There is a consistent decrease from about -10 db to -18 db over the depression angle range of 65° to 10°. Samples (a) - (c) show an upturn in slope near the upper end, and all samples show a more rapid downturn toward the lower end. With the data
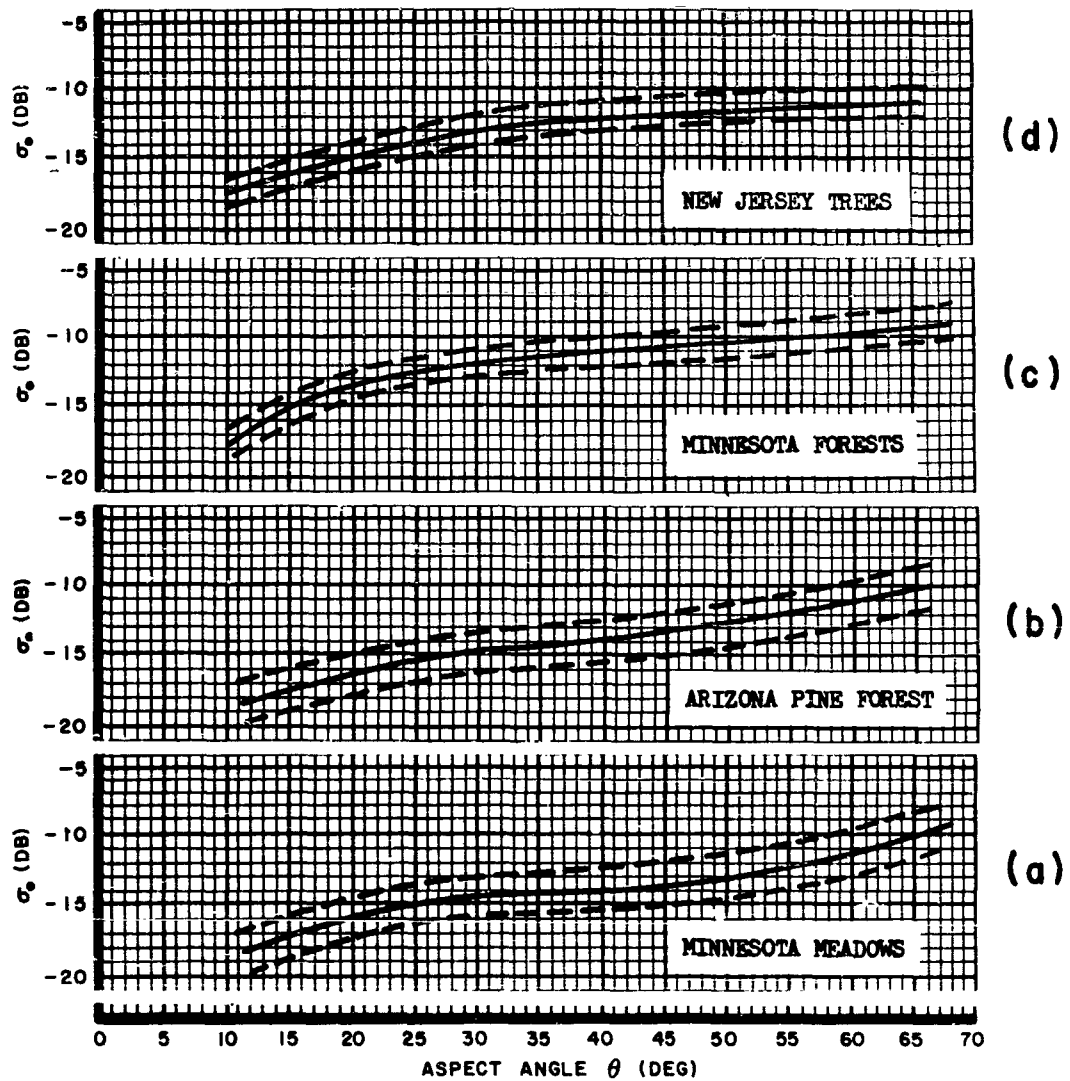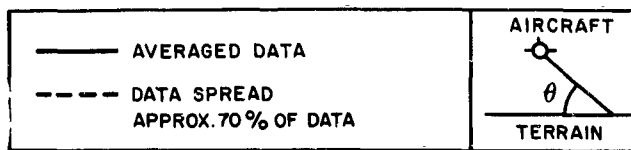
41

FIG. 3-4 σ° for various types of terrain.

spread indicated by the dashed lines, it would not be possible to draw definite conclusions regarding the significance of these trends.

Fig. 3-5 is another four-sample composite, embracing a somewhat wider variety of terrain, ranging from swamp to desert, and including cultivation. Samples (a) and (d) resemble those in Fig. 3-4 in form, but lie about 2 db higher in level. Sample (b) (New Jersey Marsh) is almost identical to sample (d) in Fig. 3-4 (New Jersey trees). Sample (c) (Arizona Desert), on the other hand, shows a distinctly different shape, the curve being concave upward throughout, and varying over a much wider range -- -12 db to -30 db.

In contrast to Figs. 3-4 and 3-5, Fig. 3-6 shows some striking features. The steep decrease below 10°, the minimum at an angle of $2^\circ - 4^\circ$, and the sharp rise toward 0° all appear unusual enough to suggest that they have some important physical significance. Before offering an interpretation of these features, however, the reader is asked to mask temporarily the portion of Fig. 3-6 below 10° with a sheet of paper. Now if the part of the figure which remains in view is compared with the two preceding figures, the following conclusions become apparent: Sample (c) is quite similar in shape to most of the previous samples, and differs from them only by a few db in level; samples (a) and (b) show significantly more of a downturn at the small depression angle end. However, if the measurements did not extend below 10°, one could at best only conjecture as to the significance of this more rapid downturn. In fact, any significance attached to it logically would have to be extended to all the curves in Figs. 3-4 and 3-5, (except possibly (c) in 3-5), since it could be argued that the downturn exists in each case, and that any difference is one of degree only.

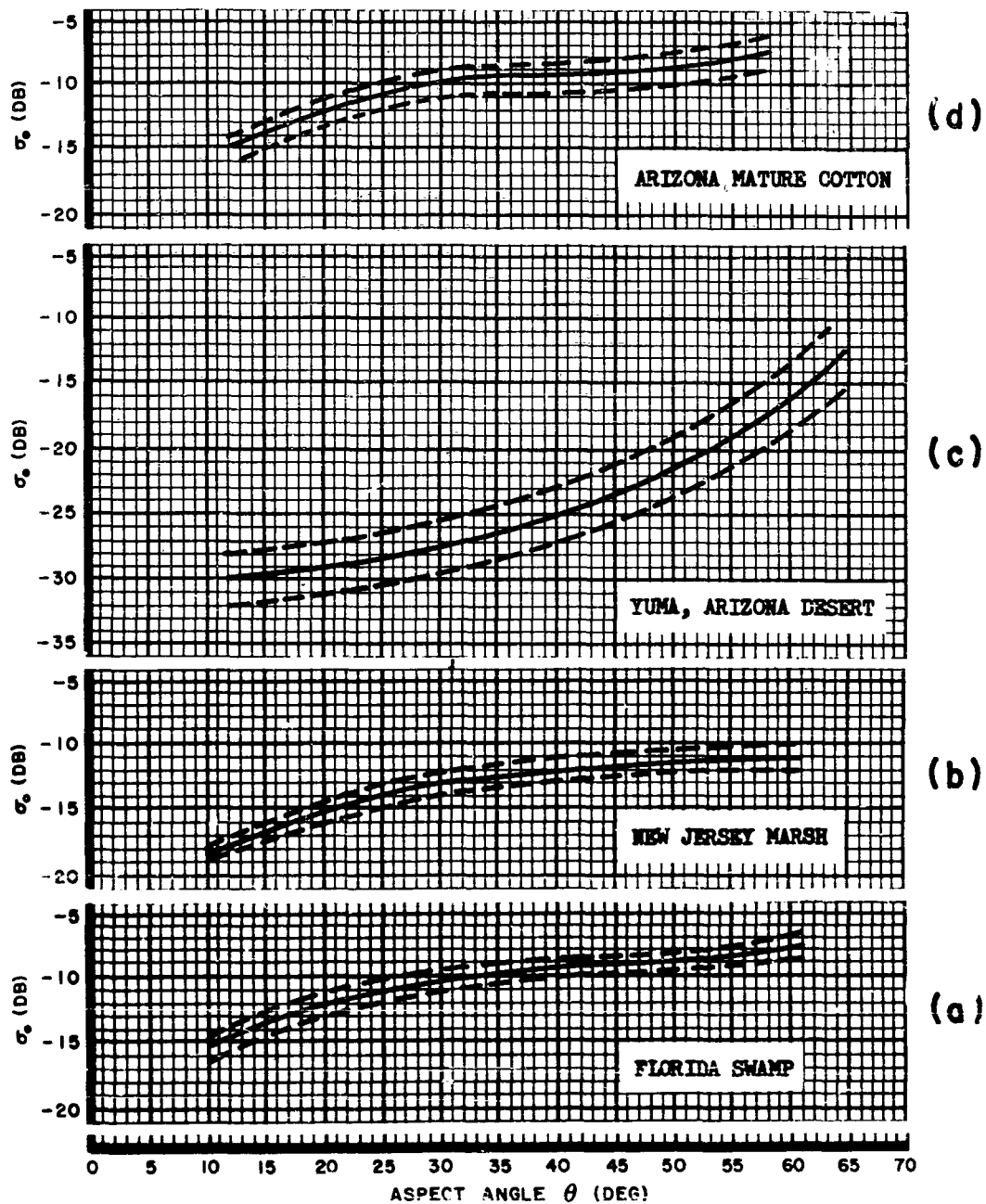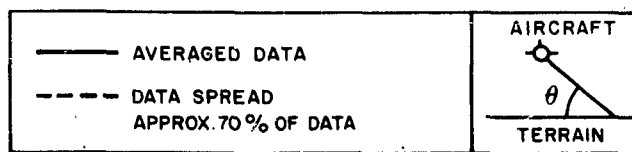If now the mask over the portion of Fig. 3-6 is removed, then the fol-

43

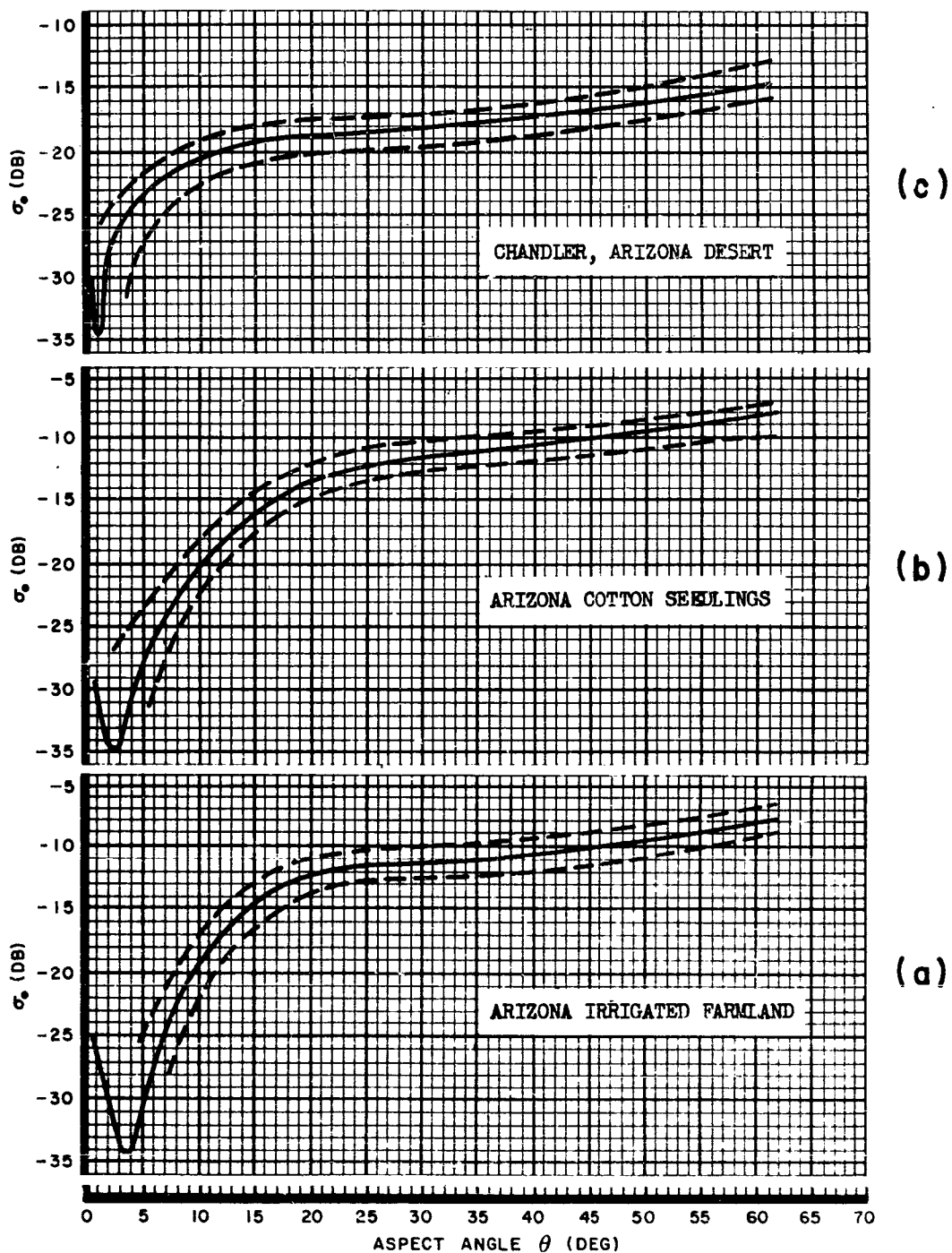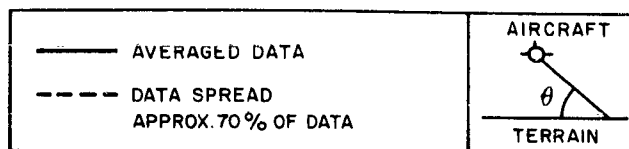FIG. 3-5 σ° for various types of terrain.

44

FIG. 3-6 σ' for various types of terrain.

lowing facts can be deduced. In (a), for example, the portion just to the right of the minimum increases very closely as $\sin^4\theta$, since from 4° to 8° the curve rises from -34 db to -22.3 db, or 11.7 db (a $\sin^4\theta$ increase would require a rise of 12.08 db). But this is strongly suggestive of the reflection interference phenomenon (see (2.13) and (2.16)), which would lead to a $\sin^4\theta$ variation at small values of θ.

A logical explanation for the rise to the left of the minimum is not difficult to find. A vertical cylinder will back-scatter most strongly at horizontal incidence (horizontal polarization gives substantially the same amplitude as vertical polarization if the cylinder has a diameter of at least $\lambda/4$, which, in this case, is about 0.3 inch). If the cylinder were not exactly vertical, the angle of maximum scattering would be shifted accordingly. A collection of cylinders with axes distributed over a certain range about the vertical then would give a broadened pattern relative to that of a single cylinder.

Thus, as grazing incidence is approached, two opposing tendencies come into play. The combination of these logically leads to a minimum at some intermediate angle.

For sample (b) of Fig. 3-6, a similar behavior is evident, except that the rise from 3° to 6° is only 8.5 db instead of 12 db as required by a $\sin^4\theta$ dependence. In sample (c), the minimum occurs at 1°, and the curve is characterized by a much sharper rise either side of the minimum. Here it is possible to draw a $\sin^4\theta$ dependence on the upper side without difficulty within the confidence limits of the data.

Having thus offered a plausible explanation for the striking features of the lower ends of the curves, one can then turn to the upper ends and ask

whether the slight upturn has a significance relative to a possible equally
striking behavior near vertical incidence. Of course, it is not possible, in
the absence of measurements, to make a conclusive statement regarding this
point. But the results of Yaplee and Grant [8], shown in Sec. 3.3.1, and sea
clutter measurements, indicate that a sharp rise to a maximum at vertical
incidence is quite possible, especially for marsh or swamp land.

The data in Figs. 3-4 — 3-6 are for horizontal polarization. What
difference, if any, would be expected for vertical polarization? As an in-
dication, the following evidence can be cited: On the basis of a theory due
to Rice [10], Peake [11] has shown that the back-scattered power is related
to the electrical constants of the surface, with vertical polarization giving
a stronger return than horizontal polarization, especially at small depression
angles. Measurements by Taylor [12] over slightly rough surfaces, have given
results in fair agreement with this theory. On this basis, therefore, it
would be expected that vertical polarization would yield somewhat higher and
flatter curves than those shown in Figs. 3-4 — 3-6.

To check this inference, Fig. 3-7 shows the result of measurements
on both horizontal and vertical polarization taken by NRL over New Jersey
trees [2]. Contrary to the above statement of expectation, there is no dif-
ference (within measurement accuracy) between the two polarizations. As in
the previous figures, there is a steepening drop-off at the small depression
angle end. Also, there is a rise of several decibels at 90°, indicating a
small amount of facet-type of scattering. Of perhaps greater significance,
however, is the fact that the level of the curve is about 5 db higher than
the comparable curve in Fig. 3-4(d). Whether this difference is genuine, or
represents a difference in calibration accuracy of the two systems used in

47

RADAR CROSS SECTION
NEW JERSEY WOODS
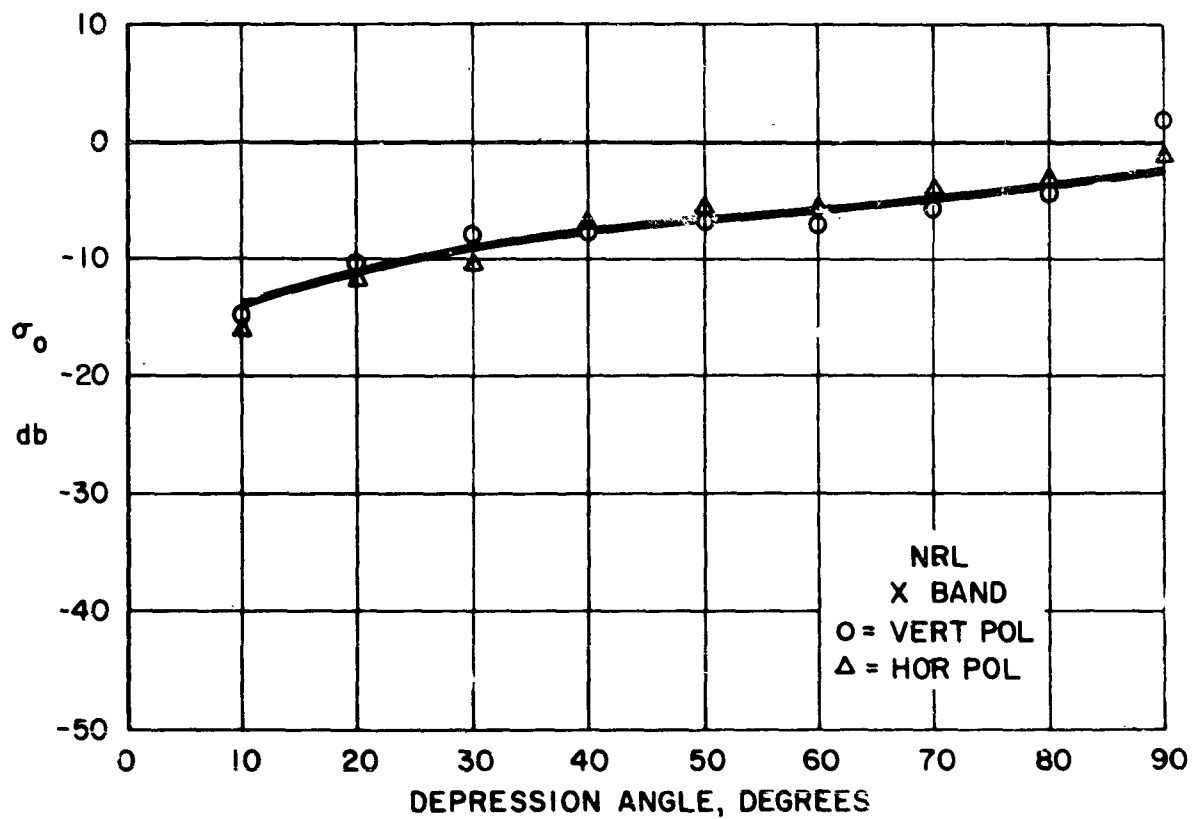
FIG. 3-7

Comparison of horizontal and vertical polarization for tree-covered terrain.

taking the measurements cannot be answered here.

The lack of polarization dependence revealed by Fig. 3-7, yet the distinct polarization dependence shown in Taylor's results referred to above, show that the nature of the polarization dependence is not clear, a distinct dependence being found in some cases, and in other cases none. The physical reasons for this behavior need to be determined.

3.4 Summary.

Ground clutter measurements show the following characteristics:

(1) Wet ground gives a stronger return than the same ground when dry.

(2) A strong specular-type return is found at vertical incidence when flat or wet patches are present.

(3) At sufficiently small elevation angles, a steep decrease with decreasing angle has been observed. This is suggestive of a reflection interference phenomenon.

(4) An enhanced return at grazing angles has been observed over vegetated areas. This may be due to the preferentially vertical extent of the vegetation.

(5) The dependence of the return on polarization is not understood. In the absence of vegetation, or with only a light vegetation cover, vertical polarization gives a stronger return, especially at small depression angles, while a heavy vegetation cover apparently leads to no polarization preference.

4. POLARIZATION PROPERTIES OF RADAR TARGETS.

Although the majority of radars transmit and receive linearly polarized waves, other polarizations are found to be advantageous for certain purposes. The use of circular polarization, for example, reduces rain clutter considerably. A full understanding of the polarization properties of targets and the potentialities of a generalized polarization of the radar antenna is not as widely known as it should be. This apparently is due in part to the preponderant use of linear polarization in practice, and in part to the use of power relations in the radar equation, in which the concept of the <u>radar cross section</u> of the target is used. In this section, a basic description of the radar process in terms of fields will be introduced, which deals with and preserves the vector nature of the phenomena. This leads to the concept of the <u>radar length</u> of the target. This is a tensor quantity. In terms of the radar length the powerful <u>polarization theorem</u> follows quite simply. The calculation of the radar length tensor for small circular disks then will be given, and the results of calculations for certain ranges of orientations will be shown for illustration.

4.1 The Radar Length Tensor.

In developing the scattering properties of a target by boundary value methods, it is necessary to deal with the field vectors, rather than with power densities. The far field of a transmitter which is incident on a target at a range R under free-space propagation conditions is given by

$$E_i = E_o \frac{e^{-ikR}}{R},\qquad(4.1)$$

where a time factor $e^{i\omega t}$ is implied, $k = 2\pi/\lambda$ and E_o is the <u>field-at-unit-distance</u> (peak value)

$$E_o = \sqrt{60PG},$$

50

P being the radiated power and G the antenna gain in the direction of the target. For other than free-space propagation conditions, the modification of the field can be represented by multiplying the right-hand side of (1) by a factor F, called the propagation factor. This is a complex quantity, or phasor, which represents the modification, in amplitude and phase, of the free-space field by the actual propagation process. (4-1) then becomes

$$E_i = E_o F \frac{e^{-i k R}}{R} .$$
(4.2)

F may be a function of the range and other parameters of the particular problem. The reflection interference phenomenon discussed in Sec. 2.1 is an example which may be cited where the presence of a reflecting surface modifies the free-space propagation relations. The factor F used there is exactly that which appears in (4.2) above.

For many purposes it is convenient and useful to consider a restricted portion of the spherical wave (4.2) as a plane wave. This is permissible if the variation of the range R over such a region results in a negligible variation of the phase $k R = 2\pi R/\lambda$, and if the propagation factor F has a negligible variation in amplitude and phase over the confines of the region. This is usually the case for airborne targets, especially at long range.

The field incident on a target sets up a current distribution therein which produces the back-scattered field of interest. Since this back-scattered field is proportional to the incident field, and since in the traverse from target to radar the same propagation phenomena are encountered as from radar to target, the field strength of the echo received by the radar is

51

$$E_r = (\ell E_i) F \frac{e^{-jkR}}{R}$$

$$= \ell E_o F^2 \frac{e^{-j2kR}}{R^2}, \tag{4.3}$$

in which the constant of proportionality ℓ is called the <u>radar length</u> of the target. This is a phasor, which represents the ratio, in amplitude and phase, of the far-field component of the back-scattered field at unit distance from the target to the incident field. The radar length is related to the more familiar radar cross section (or radar area), σ, by

$$\sigma = 4\pi |\ell^2|. \tag{4.4}$$

The radar length and radar area depend on the polarization of the incident wave. A long thin wire is a good example, since its reflectivity is very small when the incident field in linearly polarized at right angles to the wire axis, and maximum when parallel to the axis. For targets of complex shape, the total field strength incident at a given point of the target is the resultant of the primary field from the radar and the scattered fields from other parts of the target. For targets which are inclined to the wave front, the scattered field will have a component of polarization orthogonal to that of the primary field. This will be seen from the derivation of the radar length for an inclined disk which will be carried out below in Sec. 4.3. Consequently, in general, the back-scattered field has a different polarization than the incident field. The coupling between the incident and scattered polarizations depends on the incident polarization itself. As a result, the radar length is a tensor quantity, which may be written in matrix form as

$$\ell = \begin{pmatrix} \ell_{11} & \ell_{12} \\ \ell_{21} & \ell_{22} \end{pmatrix}, \tag{4.5}$$

in which each of the components ℓ_{11}, etc., is a phasor. For example, if the 1-polarization is horizontal and the 2-polarization is vertical, ℓ_{11} is the radar length of the horizontally-polarized component of the echo from a horizontally-polarized radar, ℓ_{12} is the radar length of the horizontally-polarized component of the echo from a vertically-polarized radar, etc. By reciprocity, $\ell_{12} = \ell_{21}$ for targets composed of isotropic materials.

Since any state of polarization of the incident wave may be described in terms of two orthogonal polarizations, an arbitrarily polarized incident wave may be denoted by the matrix

$$E_i = \begin{pmatrix} E_1 \\ E_2 \end{pmatrix},$$

in which, of course, the orthogonal components E_1, E_2 are phasors. The back-scattered field-at-unit distance then is given by

$$E_{or} = \begin{pmatrix} E_{or1} \\ E_{or2} \end{pmatrix} = \ell E_i \begin{pmatrix} \ell_{11} & \ell_{12} \\ \ell_{21} & \ell_{22} \end{pmatrix} \begin{pmatrix} E_1 \\ E_2 \end{pmatrix} = \begin{pmatrix} \ell_{11} E_1 + \ell_{21} E_2 \\ \ell_{21} E_1 + \ell_{22} E_2 \end{pmatrix} \quad (4.6)$$

4.2 The Polarization Theorem.

An interesting and powerful theorem follows direction from (4.6). For any given target and aspect, there is a polarization of incident field which gives maximum echo, and another which gives zero echo. This can be seen readily as follows: By adjustments of the radar antenna system, the ratio E_2/E_1 may be adjusted (in magnitude and phase) until the received polarization is orthogonal to that of the receiving system, so that then no signal will be received from the target. Similarly, an antenna polarization may be chosen such that the polarization of the echo coincides with that of the receiver, so that then a maximum echo will be received.

Some caution is needed in applying the above theorem, since it is possible

to build a radar which transmits one polarization, and receives, on two separate receiver channels, the transmitted polarization and its orthogonal. For such a system, the theorem applies to only one receiver channel at a time.

4.3 The Radar Length Tensor for Small Disks.

Since scattering by flat plates has been shown to be important in the clutter problem, it is of interest to examine the polarization properties of this scattering. In particular, the cross-polarized component in back-scattering will be determined. For this purpose, the matrix for the radar length tensor will be derived here for small circular disks.

The scattering of a small disk is a complementary problem to diffraction by a small hole in an infinite plane conductor. The solution of one problem may be obtained from the solution of the complementary problem by the application of the Booker-Babinet principle [13,14]. According to this principle, the solution for the disk corresponds to that for the hole with the roles of horizontal and vertical polarizations interchanged.

The diffraction of a plane wave by a small hole has been treated by Bethe [15]. Although Bethe's analysis is partly in error, this does not affect the results for the far field [16]. Since only the far field is of concern in the usual radar problem, Bethe's results are applicable, so that the Booker-Babinet principle may be applied to the Bethe solution to obtain the radar length of a small disk. A "small disk" is one whose circumference is small compared to the wavelength, so that phase variations over the disk are negligible.

With a view to the ultimate application of the results to an assembly of disks of various orientations, the results will be derived for a single disk having an arbitrary orientation with respect to a fixed coordinate system

to which the radar direction is referred. This coordinate system will be located with its xy-plane coinciding with the earth's surface (assumed plane), with the positive z-direction upward, and with the incident wave normal in the yz-plane, with a positive y-component, as indicated in Fig. 4-1. In this coordinate system, a plane wave of any polarization always may be resolved into components of any two orthogonal polarizations. These two orthogonal polarizations will be taken to be vertical and horizontal. Hence it is sufficient to calculate separately the scattered field for an incident vertically polarized wave and for an incident horizontally polarized wave.

Bethe divided his problem into two parts, one for the magnetic vector parallel to the plane of the hole (electric vector parallel to the plane of incidence) and the other for the electric vector parallel to the plane of the hole (perpendicular to the plane of incidence).

For an arbitrary orientation of the disk to the reference coordinate system, an incident vertically polarized wave, for example, will have components both parallel and perpendicular to the plane of incidence on the disk. Since the relative back-scattered amplitude is not the same for these two polarizations, the scattered wave then will be of mixed polarization, in general.

The procedure will be as follows: The incident field first will be resolved into components parallel and perpendicular to the plane of incidence on the disk. For each of these components, the polarization of the back-scattered field is the same as that of the incident field. The back-scattered components are evaluated from the Bethe solution, and then these are resolved into components parallel and perpendicular to the incident field to obtain the
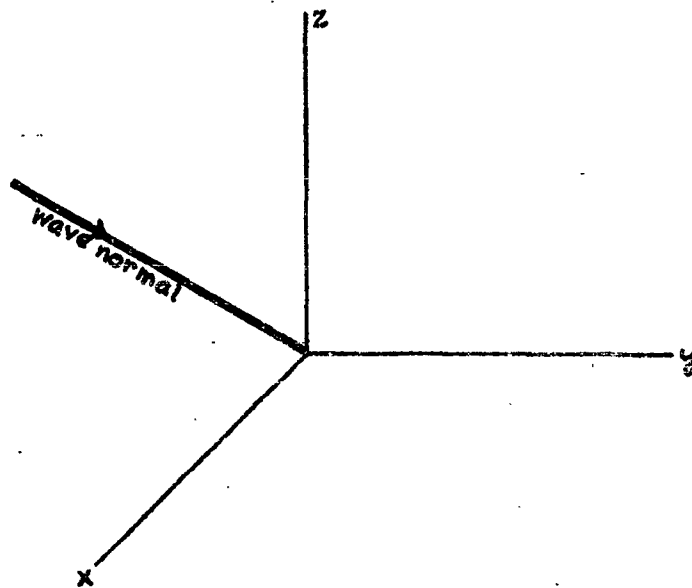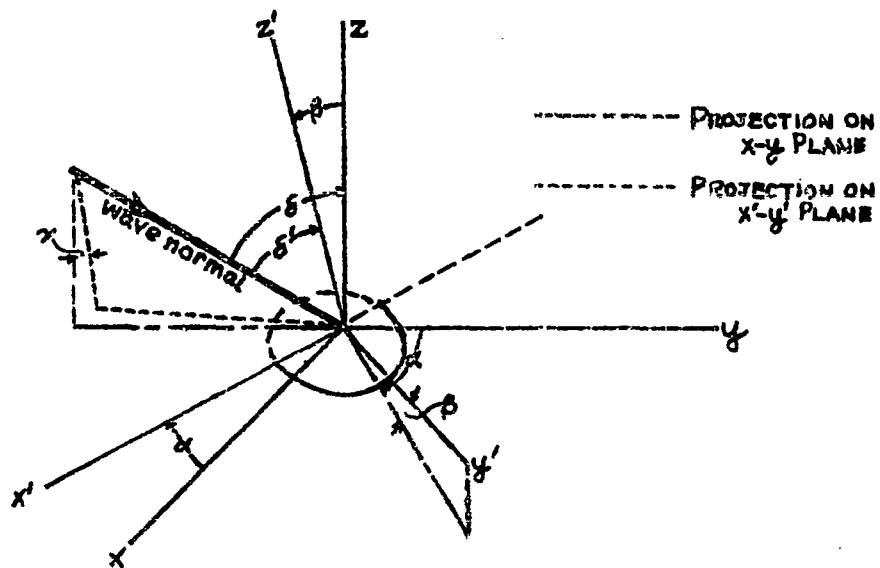
FIG. 4-1

PROJECTION ON
X-Y PLANE
PROJECTION ON
X'-Y' PLANE

FIG. 4-2

56

corresponding components of the radar length tensor. This procedure is carried out both for an incident vertically polarized field, and for an incident horizontally polarized field, so that the complete radar length tensor is obtained. The results of sample calculations then will be shown in the form of curves for various disk orientations.

Consider a circular disk with its center at the origin of the (X, Y, Z)-coordinate system. As in Fig. 4-2, define a coordinate system (x', y', z') for the disk, with the z'-axis normal to the disk and the y'-axis in the plane containing the Z- and z'-axes. Then the y'-axis is the line of steepest ascent in the disk in the (X, Y, Z)-coordinates. By symmetry it follows that the x'-axis lies in the XY-plane. Denote the angle between the Z- and z'-axes by β (this is the elevation of the facet), and the angle between the Y-axis and the projection of the y'-axis by α (which is the azimuth of the facet).

Denoting the angle of the incident wave normal to the Z-axis (i.e., the angle of incidence) by δ, the corresponding angle to the z'-axis by δ', (the angle of incidence on the facet), and the angle between the planes containing these angles by γ, then from spherical trigonometry

$$\cos\beta = \cos\delta\cos\delta' + \sin\delta\sin\delta'\cos\gamma,$$

or

$$\cos\gamma = \frac{\cos\beta - \cos\delta\cos\delta'}{\sin\delta\sin\delta'}. \tag{4.7}$$

Also

$$\sin\gamma = \frac{\sin\alpha\sin\beta}{\sin\delta'}, \tag{4.8}$$

$$\cos\delta' = \cos\beta\cos\delta + \sin\beta\sin\delta\cos\alpha. \tag{4.9}$$

From the Bethe analysis, the following values of radar length can be

57

deduced:

$$\ell_\perp = -2(2 + \sin^2 \delta') \cdot C \tag{4.10}$$

$$\ell_{||} = -4 \cos^2 \delta' \cdot C \tag{4.11}$$

where

$$C = \frac{1}{3\pi} k^2 a^3 = \frac{4\pi}{3\lambda^2} a^3 \tag{4.12}$$

a = disk radius.

The subscripts $\perp$ and $||$ indicate that the incident electric vector is perpendicular or parallel to the plane of incidence on the facet.

(a) Vertical Polarization.

An incident vertically polarized (in the $X\,Y\,Z$ -system) field E_V has the two components in the facet $(X'Y'Z')$ coordinates

$$E_{||} = E_V \cos \gamma,$$
$$E_\perp = E_V \sin \gamma,$$

and these give rise to back-scattered components

$$E'_{||} = \ell_{||} E_{||} = \ell_{||} \cos \gamma E_V,$$
$$E'_\perp = \ell_\perp E_\perp = \ell_\perp \sin \gamma E_V,$$

respectively. These then combine to give the back-scattered components

$$E'_V = E'_{||} \cos \gamma + E'_\perp \sin \gamma = (\ell_{||} \cos^2 \gamma + \ell_\perp \sin^2 \gamma) E_V,$$
$$E'_H = E'_\perp \cos \gamma - E'_{||} \sin \gamma = (\ell_\perp \sin \gamma \cos \gamma - \ell_{||} \sin \gamma \cos \gamma) E_V.$$

Hence

$$\ell_{22} = E'_V / E_V = \ell_{||} \cos^2 \gamma + \ell_\perp \sin^2 \gamma$$
$$= -(6 \sin^2 \gamma \sin^2 \delta' + 4 \cos^2 \delta') C$$
$$= -[6 \sin^2 \alpha \sin^2 \beta + 4(\cos \beta \sin \theta \tan \beta \cos \theta \cos \alpha)^2] C \tag{4.13}$$

58

$$l_{12} = E'_H/E_V = (l_\perp - l_{||})\sin\gamma\cos\gamma$$
$$= -6\sin^2\delta\sin\gamma\cos\gamma\, C$$
$$= -6(\cos\beta\cos\theta - \sin\beta\sin\theta\cos\alpha)\sin\alpha\sin\beta\, C \quad (4.14)$$

(b) Horizontal Polarization.

An incident horizontally polarized field E_H has the two components in the facet coordinates

$$E_{||} = -E_H\sin\gamma,$$
$$E_\perp = E_H\cos\gamma,$$

and these give rise to back-scattered components

$$E'_{||} = l_{||}E_{||} = -l_{||}\sin\gamma E_H,$$
$$E'_\perp = l_\perp E_\perp = l_\perp\cos\gamma E_H,$$

respectively. These then combine to give the back-scattered components

$$E'_V = E'_\perp\sin\gamma - E'_{||}\cos\gamma = (-l_\perp + l_{||})\sin\gamma\cos\gamma E_H,$$
$$E'_H = E'_\perp\cos\gamma - E'_{||}\sin\gamma = (l_\perp\cos^2\gamma + l_{||}\sin^2\gamma)E_H.$$

Hence

$$l_{22} = E'_H/E_H = l_\perp\cos^2\gamma + l_{||}\sin^2\gamma$$
$$= -(6\cos^2\gamma\sin^2\delta' + 4\cos^2\delta')\,C$$
$$= -[6(1 - \sin^2\alpha\sin^2\beta) - 2(\cos\beta\sin\theta + \sin\beta\cos\theta\cos\alpha)^2]\,C \quad (4.15)$$

$$l_{21} = E'_V/E_V = (-l_\perp + l_{||})\sin\gamma\cos\gamma$$
$$= -6\sin^2\delta'\sin\gamma\cos\gamma\, C$$
$$= l_{12} \quad (4.16)$$

Calculations of l_{11}, l_{12} and l_{22} have been made for selected orienta-

tions of the disk. The results are shown in Figs. 4-3 — 4.6.

Fig. 4-3 shows the radar length components for back scattering in the plane of incidence (i.e., $\alpha = 0$) as a function of elevation angle of the facet (β) for a horizontally incident wave ($\theta = 0$). $\mathcal{L}_{11}$ decreases from a value $6\mathcal{L}$ at grazing incidence to $4\mathcal{L}$ at normal incidence. In contrast, $\mathcal{L}_{22}$ increases from 0 at grazing incidence to $4\mathcal{L}$ at normal incidence. $\mathcal{L}_{12}$ is zero throughout, since no cross polarization is generated in this range of aspect. In this range of orientations, horizontal polarization always gives a stronger echo than vertical polarization, except at normal incidence, where the two are equal.

Fig. 4-4 shows the radar length components as a function of azimuth angle (α) for $\beta = 30°$, $\theta = 0°$. Here horizontal polarization gives a much larger return than vertical polarization, the ratio of the two varying between 14.8 and 9.5 db with azimuth. It is interesting to note that the cross polarized component is 4.8 db stronger than the vertically polarized component at $\alpha = 90°$ (that is, for an incident vertically polarized wave, the horizontally polarized echo is stronger by 4.8 db than the vertically polarized echo).

Fig. 4-5 shows similar results for $\theta = 30°$, $\beta = 30°$. The ratio $\mathcal{L}_{11}/\mathcal{L}_{12}$ now is only about 1.5 (~ 2 db) for $\alpha < 90°$. $\mathcal{L}_{12}$ exceeds $\mathcal{L}_{22}$ only for $\alpha > 90°$.

Fig. 4-6 shows an interesting case where $\mathcal{L}_{22}$ before a considerable range of α. The ratio is in the order of 10 db for an appreciable range of α. It is interesting also that $\mathcal{L}_{22}$ rises to larger values than the maximum value when the plane of incidence is normal to the faces (see Fig. 4-3). The cross polarized component $\mathcal{L}_{12}$ now also exceeds $\mathcal{L}_{11}$ for the first time.

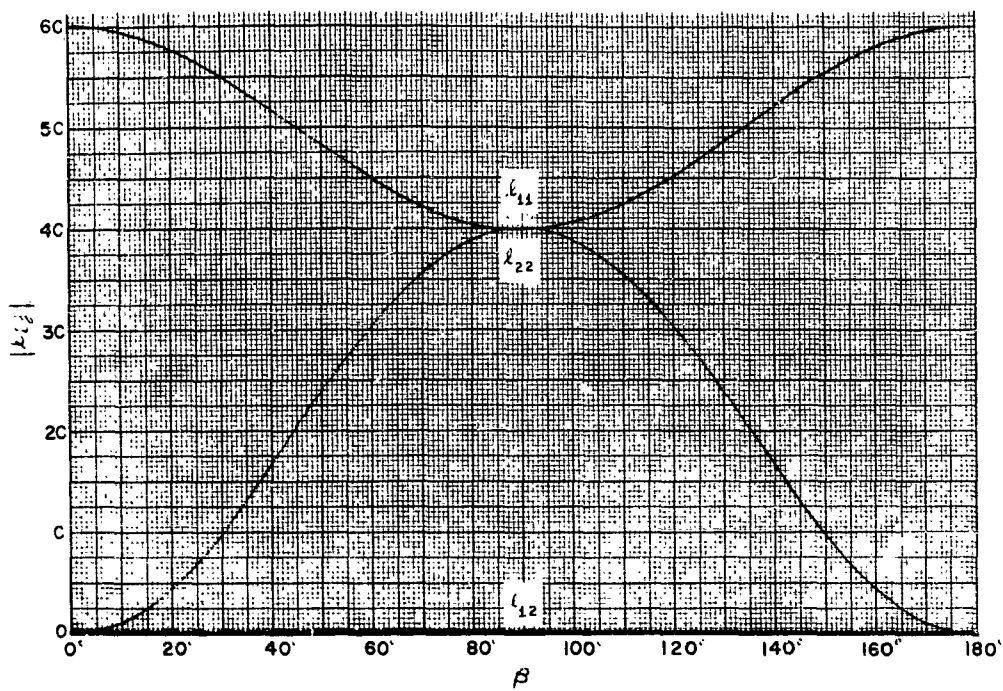The conditions represented in Fig. 4-6 are of the right order to explain
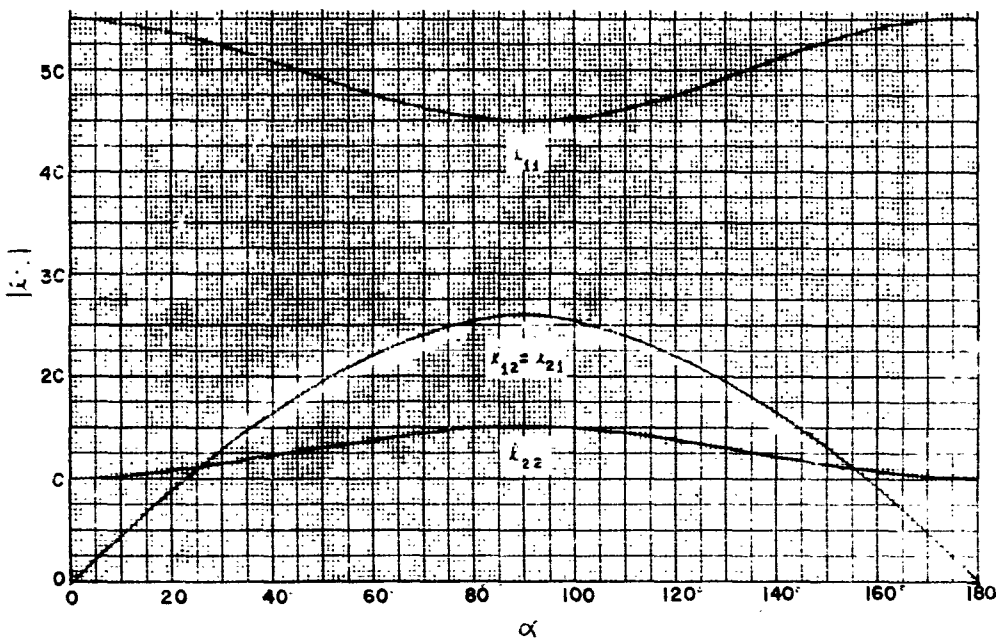
FIG. 4-3   Components of the radar length tensor

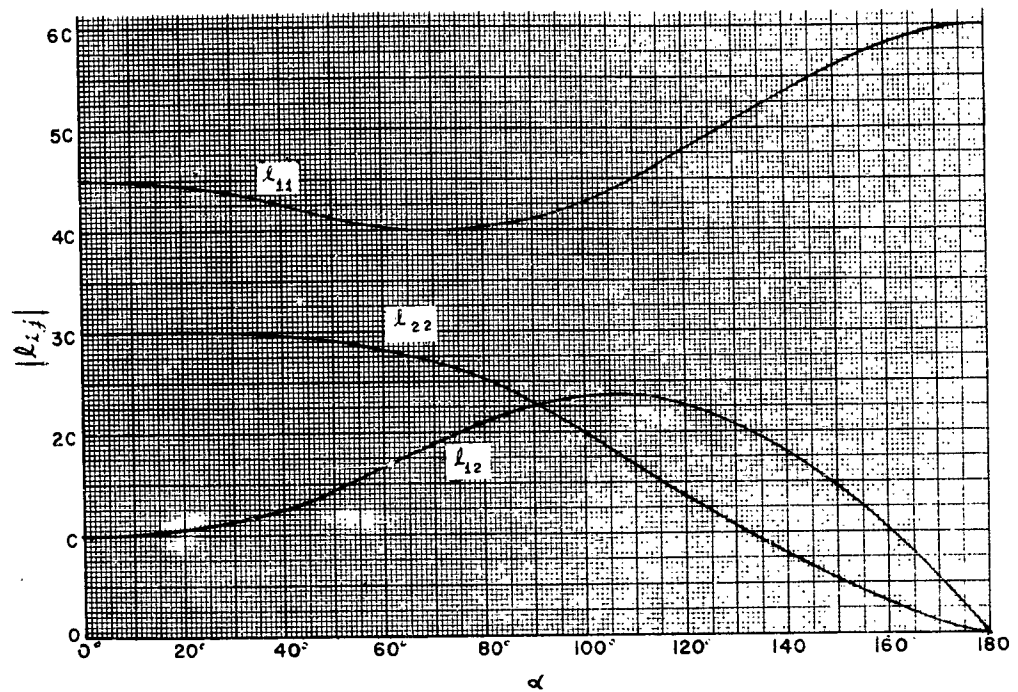

FIG. 4-4   Components of the radar length tensor

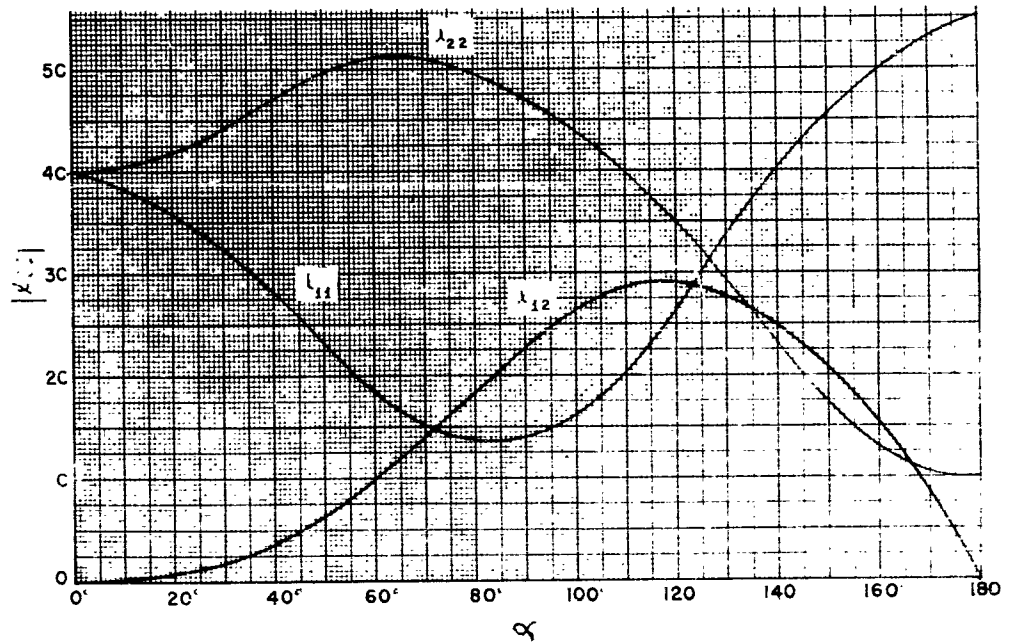FIG. 4-5   Components of the radar length tensor

FIG. 4-6   Components of the radar length tensor

62

the unusual polarization characteristics noted in Fig. 2-12. The required properties are exhibited in the neighborhood of $\alpha = 90°$. This indicates that the facets of the cross-sea waves are the ones that contribute most prominently to the vertically polarized return, as well as to the cross polarized return. The fact that the required behavior is available in the polarization characteristics of small facets indicates also that the clutter in the region in question is due mainly to small facets. This conclusion also is reached from a consideration of the angular distribution of $\sigma°$ [12].

Fig. 4-4 may be taken to be representive of the behavior for very small depression angles. For smaller values of β, the $\mathcal{L}_{22}$ curve is shifted downward by the factor $\sin^2\beta$, while the $\mathcal{L}_{11}$ curve is lifted non-uniformly by a small amount, resulting in a smaller range of variation with α. For $\beta = 15°$, for example, the ratio $\mathcal{L}_{11}/\mathcal{L}_{22}$ becomes about 30 db. Since the facet slope β becomes very small in a calm sea, it can be seen quite readily that vertical polarization will produce a much smaller return for a given strength of illuminating field than will horizontal polarization. But in Sec. 2 it was shown that reflection interference resulted in a much stronger illumination of the scattering elements (at very small depression angles) with vertical polarization than with horizontal polarization. The two effects (scattering and illumination) work in opposite directions, the latter tending toward a limiting value, while the former decreases toward zero. Consequently, for a smooth sea an angle of crossover eventually will be reached, below which the return on vertical polarization is less than that on horizontal polarization. This behavior, however, would appear only in a calm sea, where the maximum value of β is not large. It is interesting to note that the measurements shown in

63

Fig. 2-10 were made in sea state 1, which is quite a calm sea.

It would be desirable to extend the calculation of the radar length tensor to larger disks, whose circumference is comparable to the wavelength, since the facet theory indicates that these are the most effective back scatterers for small depression angles. Unfortunately, the calculations become very involved, since the solution is in terms of a rather slowly converging series [17,18]. For this reason, we have investigated an alternative approach along the lines of the comparable problem in scattering by spheres, for which we have derived an exact solution [19]. This investigation has not been completed, however, so that no results are available at this time.

64

5. COHERENT RADAR MEASUREMENT SYSTEMS.

The results of Sec. 4 point out the importance and desirability of
knowing the full polarization properties of the back scattering by ground
areas. From the experience gained from sea clutter investigations, it is
likely that the features observed in experimental measurements may lead to
the identification of important physical processes in ground clutter, re-
sulting in a better understanding of the phenomenon, and the ability to ap-
ply this understanding to practical problems. Consequently, it is eviden'
that the accumulation of data on the polarization properties of ground clutter
is desirable. Recommendations for a specific measurement program designed
for the Maynard field site radar already have been submitted under this con-
tract [1].

In this section, the principles of direct measurement of the radar length
tensor will be discussed, and the advantages of a coherent radar for making
such measurements will be pointed out. Details will be given for a coherent
pulse radar for use in measurements of the radar length tensor (sometimes re-
ferred to as the polarization matrix). In particular, a new calibration
technique will be described whereby such measurements may be placed on a
quantitative basis.

Measurement systems which have been described heretofore can be classi-
fied into two general categories, continuous-wave (cw) systems, and pulse
systems [20- 23]. In a cw system, reflections from the surroundings are
balanced out by a component derived from the transmitted signal. The amount
of unbalance which occurs when the target is placed within the radar beam
then is a measure of its reflectivity. Pulse systems discriminate between

65

target and background by using the pulse duration to control the region illuminated. Almost without exception these systems are designed to measure the radar area (the ratio of received to transmitted power) of the target. Although some of the systems measure this power ratio for different combinations of transmitted and received polarizations, practically none of the systems measures the relative phase of the received and transmitted fields (we recently have learned of one exception). Consequently, to obtain a complete measurement of the back-scattering properties of the target it is necessary to make at least five separate measurements with five different incident polarizations. The coherent back-scattering measurement system described in this section, in contrast, is designed to measure the complete radar length tensor by measuring both the amplitudes and phases of the two orthogonal components of the back-scattered field. Then two sets of measurements, with only two different incident polarizations, are sufficient to determine the complete radar length tensor of the target.

The principle of measuring both amplitude and phase of the target reflection also may be applied to c-w systems. However, this does not allow the use of an absolute calibration technique such as that which will be described in connection with the pulsed system.

5.1 Principle of Measurement.

The principle on which the measurement of the radar length tensor is based may be explained in terms of equations (4.3) and (4.6). These may be combined to form the following expression for the received field

$$E = \begin{pmatrix} E_{\eta_1} \\ E_{\eta_2} \end{pmatrix} = \mathcal{L} \begin{pmatrix} E_{A_1} \\ E_{A_2} \end{pmatrix} F^2 \frac{e^{-j2\Delta R}}{R^2},$$

$$= \begin{pmatrix} \ell_{11} E_{A_1} + \ell_{12} E_{A_2} \\ \ell_{21} E_{A_1} + \ell_{22} E_{A_2} \end{pmatrix} F^2 \frac{e^{-j2\Delta R}}{R^2}$$

(5.1)

66

in which $\begin{pmatrix} E_{x_1} \\ E_{x_2} \end{pmatrix}$, in general, is the elliptically polarized transmitted field-at-unit-distance. This may be written in a more general form than (4.1a) as follows:

$$\begin{pmatrix} E_{x_1} \\ E_{x_2} \end{pmatrix} = \sqrt{60P} \begin{pmatrix} \sqrt{G_1} \\ \sqrt{G_2}\, e^{i\varphi} \end{pmatrix}, \qquad (5.1a)$$

where G_1 and G_2 are the antenna gains for the two components, and φ is the phase difference between the corresponding field components. For example, if the two orthogonal polarizations 1 and 2 are chosen to be horizontal linear and vertical linear, then $G_1 = G_2$, and $\varphi = 0$. Hereafter, to simplify the discussion, it will be assumed that $G_1 = G_2 = G$. The extension to the general case should be obvious.

Providing the propagation factor F is identical for both polarizations, (5.1) may be written as the two equations

$$E_{r_1} = K \left(\ell_{11} E_{x_1} + \ell_{12} E_{x_2} \right),$$
$$E_{r_2} = K \left(\ell_{21} E_{x_1} + \ell_{22} E_{x_2} \right),$$

in which K is the complex constant (for a fixed range R)

$$K = F^2 \frac{e^{-i 2\beta R}}{R^2}. \qquad (5.2)$$

By making $E_{x_2} = 0$ (i.e., transmitting only the 1-component E_{x_1}), these reduce, so that

$$\ell_{11} = \frac{1}{K} \frac{E_{r_{11}}}{E_{x_1}}, \qquad (5.3a)$$

$$\ell_{21} = \frac{1}{K} \frac{E_{r_{21}}}{E_{x_1}}, \qquad (5.3b)$$

the additional subscript on E_r denoting the transmitted polarization. Next, by making $E_{x_1} = 0$ and transmitting only the 2-component E_{x_2}, there results

$$\ell_{12} = \frac{1}{K} \frac{E_{r_{12}}}{E_{x_2}}, \qquad (5.3c)$$

$$\ell_{22} = \frac{1}{K} \frac{E_{r_{22}}}{E_{x_2}}. \qquad (5.3d)$$

67

These relations may be written in the general form

$$\ell_{ij} = \frac{1}{K} \frac{E_{ri}}{E_{tj}}.$$

(5.4)

Since the ℓ_{ij} in the above equations involve only the ratio of received to transmitted fields, it is necessary to measure only amplitude ratios and phase differences of the corresponding fields. This is characteristic of all radar measurements, where it is possible to take advantage of the coalescence of transmitter and receiver terminals to obviate the necessity for absolute amplitude or phase measurements.

Each of the four radar length components has an amplitude and phase. The phase of one of these, say ℓ_{11}, may be set equal to zero by incorporating its phase in the exponential factor $e^{-j2\Delta R}$ in (5.1). Furthermore, since by the reciprocity theorem $\ell_{12} = \ell_{21}$ for isotropic materials, the separate measurement of ℓ_{12} and ℓ_{21} provides a check of the accuracy of the measurement system.

The scheme thus is to make two sets of measurements of both orthogonal components of the received field, one set for each orthogonal component of field transmitted alone. By measuring the complex ratios of received to transmitted field, the radar length components can be determined uniquely.

Since the two sets of measurements cannot be made simultaneously, there must be a difference in time between the successive measurements. This poses a problem when the target is in motion, since then the radar length may vary with time. By suitable obvious techniques, the time difference between measurements may be decreased, but not to zero.

An alternative procedure may be used if the target configuration is such that the radar length does not change rapidly with frequency. By using two

68

separate frequencies, coherently related, the two orthogonal transmitted polarizations may be emitted simultaneously, one on each frequency.

Systems based on sequential measurements on a single frequency, and on simultaneous measurements on separated frequencies, will be described below.

5.2 Sequential Measurement Configuration.

A system for measuring the radar characteristics of a target by alternately switching from one transmitted polarization to another is shown in block diagram form in Fig. 5-1. A polarizing device is connected to the antenna and operated in such a fashion that when one input to the polarizer is used to transmit and receive a given polarization, the other input line can be used to receive the orthogonal polarization. Polarizing devices that perform this function are in common use [24]. A switch is connected to the polarizer to switch the transmitter from one polarization to the other, and to switch the receivers appropriately. A duplexer is provided to isolate the receiver which responds to the transmitted polarization. The basic transmitted signal is obtained from a stable local oscillator (STALO) and a coherent oscillator (COHO). The STALO is used as the receiver local oscillator to obtain a coherent i-f signal. This i-f signal is mixed with the COHO oscillator in a phase detector to measure the relative phase between the received signal and the transmitted signal. For each transmitted polarization the receivers provide four outputs, the amplitudes and phases of each of the two received polarization components (transmitted polarization and orthogonal). Thus, by transmitting both polarizations individually, and recording the four outputs for each, the necessary eight quantities for the determination of the radar length tensor are obtained.
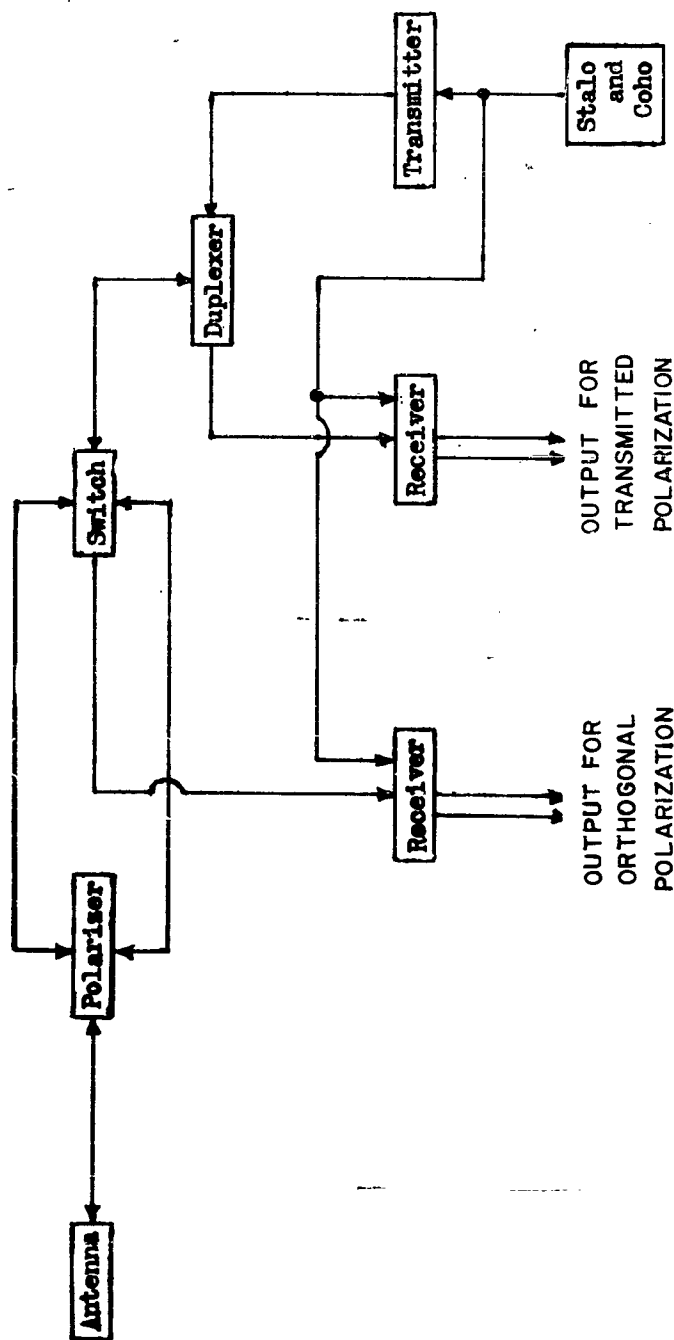
69

Transmitter

Stalo and Coho

Duplexer

Receiver

OUTPUT FOR
TRANSMITTED
POLARIZATION

Switch

Receiver

OUTPUT FOR
ORTHOGONAL
POLARIZATION

Polariser

Antenna

70

FIG. 5-1   SIMPLIFIED RADAR BLOCK DIAGRAM   (SEQUENTIAL MEASUREMENTS)

5.3 Simultaneous Measurement Configuration.

If the target characteristics change rapidly with time, the sequential measurements outlined above are inadequate if the radar length of the target has changed in the interval between the two sets of measurements. Then, providing the radar length of the target is not a rapidly varying function of frequency, it is possible to make simultaneous measurements on two slightly different frequencies with a measurement system such as that shown in the block diagram of Fig. 5-2. A polarizer is connected to the antenna to provide two polarizations as in the sequential measurement system. Two transmitters are connected to one polarizer input through a diplexer and a duplexer, and two receivers for each polarization are connected to diplexers to provide four output signals (amplitude and phase at both frequencies) for each polarization, giving a total of eight output signals. These eight signals provide the information for the radar length tensor as in the sequential system. The two transmitted frequencies can be obtained by mixing the STALO and COHO signals and using both the upper and lower sidebands. The two transmitters shown in Fig. 5-2 can be replaced by a single power amplifier transmitter if this transmitter has a bandwidth large enough to accommodate both sidebands.

The accuracy of the quantitative measurements made with the sequential and simultaneous systems described above will depend upon the accuracy of the technique used for calibration. In order to obtain optimum accuracy, a new calibration technique has been devised for this type of system. This will be described below.

5.4 System Calibration Technique.

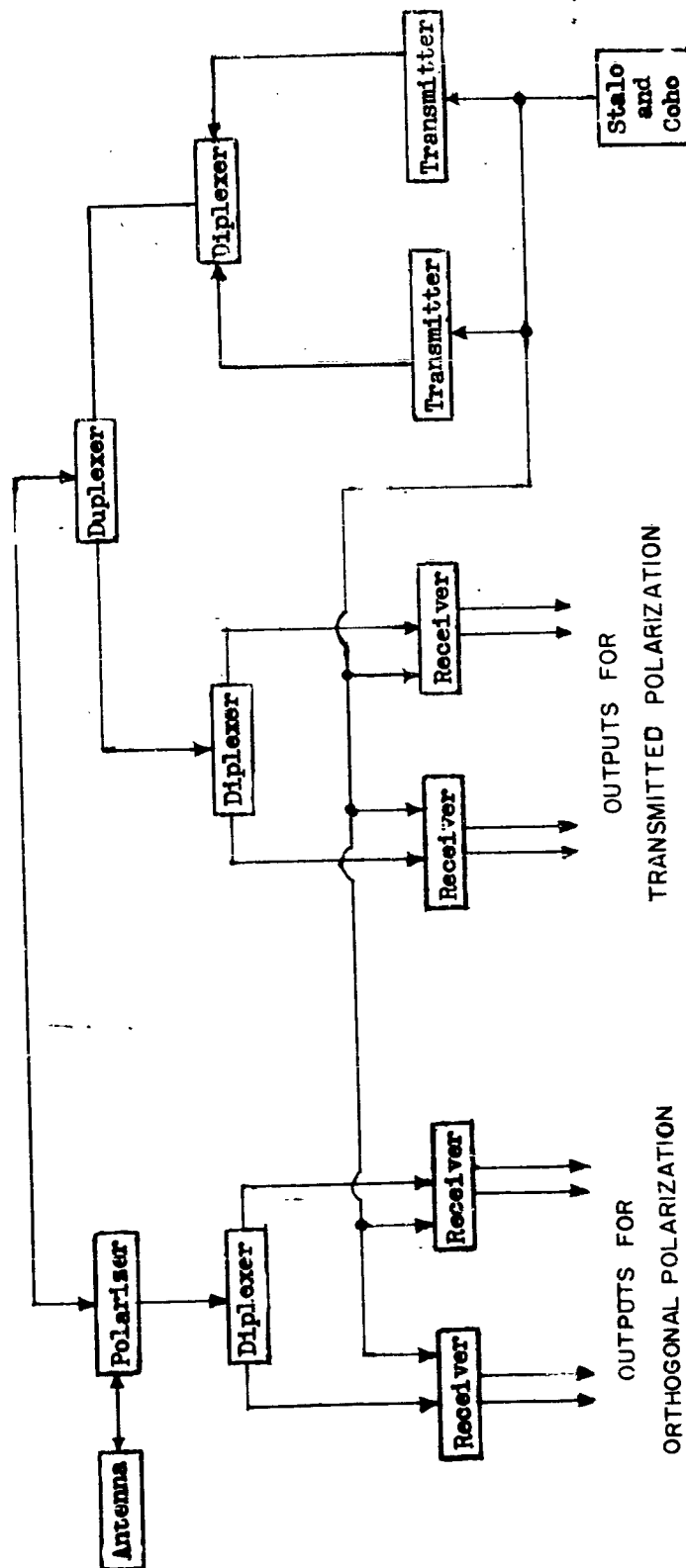From (5.4) and (5.2) it can be seen that the components of the radar

71

FIG. 5-2   SIMPLIFIED RADAR BLOCK DIAGRAM   (SIMULTANEOUS MEASUREMENTS)

72

length may be determined by measuring the complex ratios $E_{r i_j'}/E_{t_j'}$, providing the range and wavelength are known with requisite accuracy. But the $E_{t_j'}$ are the far-field components of the transmitted field, which are not readily accessible for measurement. Similarly, the $E_{r i_j'}$ are the received field strengths. Consequently, a further step is needed to relate the received and transmitted fields to voltages which may be measured at appropriate points in the radar system.

Methods of making quantitative measurements of the amplitude of this ratio (i.e., $|E_{r}/E_{t}|$) (or, equivalently, of P_r/P_t) have been reported [25,26]. The measurement technique described here, however, is capable of the measurement of the phase of this ratio as well as its amplitude. Since phase variations usually can occur more readily than amplitude variations, the calibration of the radar to measure both amplitude and phase accurately will require great care.

5.4.1 Ratio of Received to Transmitted Field.

The radar length elements are directly proportional to the complex ratio E_r/E_t of the field received at the radar to the far field transmitted by the radar. In other words, these fields are defined at the radar antenna, even though the far field of the transmitted wave is developed only at some distance from the antenna. The received signal is measured at the output of the radar receiver, which is located at some distance from the antenna, and is separated from the antenna by several intervening components, as shown in Figs. 5-1 and 5-2. The ratio of the receiver output to the field at the antenna input is influenced by such factors as the antenna gain, the phase shift through the polarizer, variations in loss and phase shift through

73

the transmission lines from the antenna to the receiver (which can be caused by temperature and humidity changes), and variations in gain and phase shift through the receiver itself. Similarly, the transmitter is separated from the antenna, so that it is necessary to determine the relationship between a voltage or field measured, say, at the transmitter, and the far-field component of the transmitted field at the antenna aperture. This, too, is affected by the various components inserted between the transmitter and the antenna, and may be affected also by such things as the input power and the frequency of operation.

Calibration of the radar for the measurement of E_p/E_x is an operation which should be performed rather frequently, because of the large number of components in the system whose transfer characteristics can be expected to vary. For convenience, it is desirable to perform this calibration at the radar operator's position. A method is described here whereby this can be accomplished.

In this method, signals of known amplitude and phase relative to the transmitter are produced in a standard antenna placed in the far field of the radar. The relative amplitude and phase of these signals are determined by comparison with the transmitted signal at the radar operator's position. This comparison actually is effected through intermediate comparisons with a locally generated reference ("signal generator"), which thereafter is used as the reference for the measurement of target signals. The measurement of the calibration signals is affected by the same transmitter and receiver transfer constants as the target signals, so that these transfer constants cancel out when the ratio is taken of target to calibration signals.

The calibration scheme is illustrated in Fig. 5-3. The transmitted pulse is received in the calibration antenna, passed through a delay network, and then back into the antenna. The delayed signal passes into a divider network, which sends a part out through the calibration antenna and thence back to the radar, and a part back into the delay network again. This process repeats over and over, so that for each transmitted pulse a series of equally spaced pulses is received at the radar from the calibration antenna. The relative amplitude and phase of any two successive pulses is the same, being determined by the characteristics of the circulation path. Consequently, a known set of ratios of E_r/E_t is produced at the radar antenna. At the same time, these known ratios will provide a calibration of the radar receivers, so that it will be possible to interpret the receiver output in terms of a ratio E_r/E_t. Thus the calibration scheme described is a logical extension and generalization of the self-calibrating scheme described earlier for non-coherent radars [26]. The calibration equipment will be explained in greater detail in Sec. 5.4.2.

The complete calibration is performed by measuring the ratios of voltages at various points in the radar system. The reference used in measuring the various fields is a signal derived from the serrodyne which excites the transmitter power amplifier.

During back-scattering measurements, as indicated in Fig. 5-4(a), the transmitter field, E_{to}, is measured by comparison with the signal generator, while the received field, E_{ro}, is recorded. During primary calibration the transmitter output is monitored while the received signal is recorded, as shown in Fig. 5-4(b). For this case the ratio of received to transmitted fields at the antenna is given by
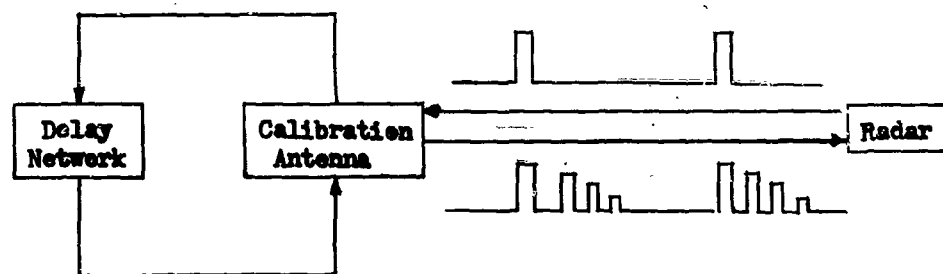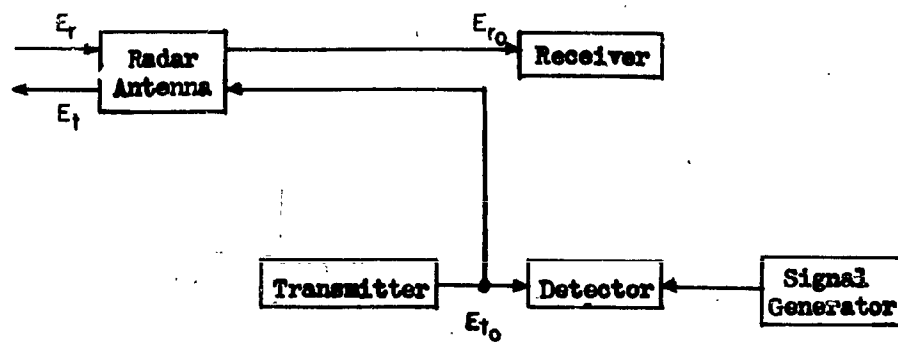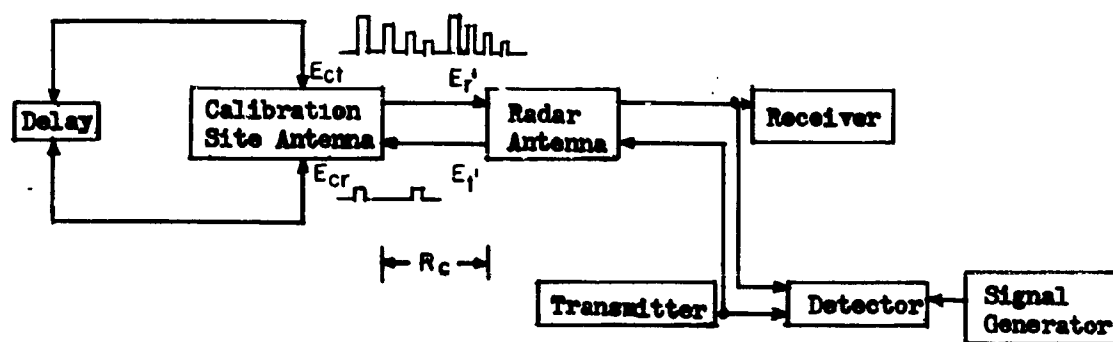
FIG. 5-3   SELF-CALIBRATION SCHEME

76

(a) SIGNAL FLOW DURING BACK-SCATTERING MEASUREMENT

(b) MEASUREMENT OF RATIO OF SUCCESSIVE PULSES RETURNED FROM CALIBRATION SITE

FIG. 5-4   SIGNAL FLOW FOR CALIBRATION

77

$$\frac{E'_r}{E'_t} = \left[\frac{E_r}{E_{ct}}\right]\left[\frac{E_{ct}}{E_{cr}}\right]\left[\frac{E_{cr}}{E_t}\right] \qquad (5.5)$$

where E_{cr} and E_{ct} are the received and re-transmitted (far) fields at the calibration antenna, respectively. If we denote the free-space transmission coefficient between the radar and the calibration antenna terminals by w_{fs}, then

$$\frac{E'_r}{E'_t} = w_{fs}^2\left[\frac{E_{ct}}{E_{cr}}\right] = w_{fs}^2 \, w_c \, , \qquad (5.6)$$

where $w_c = E_{ct}/E_{cr}$ is a quantity which can be determined by a calibration, and

$$w_{fs}^2 = \left(\frac{\lambda}{R_c}\right)^2 \frac{G_c}{4\pi} \cdot e^{-j2kR_c} \, , \qquad (5.7)$$

R_c being the separation between radar and calibration antennas, and G_c the gain of the calibration antenna.

The key to the accurate calibration of the ratio E_r/E_t obtained from a target is the ability to establish a known ratio E'_r/E'_t at the radar antenna by use of the calibration equipment. From eq. (5.6) it can be seen that a knowledge of the transmission coefficient of the calibration equipment, w_c, and the transmission coefficient w_{fs} is required. Since w_{fs} involves stable quantities, its determination poses no unusual problems. The calibration equipment, however, contains amplifiers and other components whose characteristics may be expected to vary, so that the transmission coefficient of this equipment should be measured during the calibration procedure.

The ratio w_c is obtained by measuring two successive pulses returned to the radar from the calibration equipment, again using the signal generator as a reference for each, as shown in Fig. 5-h(b). With w_c thus determined, the successive pulses define known points on a calibration curve of received field versus E_r/E_t. As part of the measurement routine, the radar should be pointed

78

at the calibration equipment before and after each measurement, and the ratio w_c determined.

In the above measurements, it is necessary to compare the serrodyne exciter (serving as a signal generator) with signals which occur at different times. This can be accomplished by pulsing the exciter after the "main bang" at the instant the signal to be measured occurs. Consequently, a delayed pulse whose timing can be controlled is required for the exciter.

Obviously, to obtain accurate measurements of the ratio E_r/E_t requires the use of accurate and reliable calibration equipment.

5.4.2 Calibration Equipment.

As described above, a calibration is needed to determine the ratios E_{rij}/E_{tij}. The calibration procedure has been explained above in Sec. 5.4.1. This procedure requires the measurement of the transmitted and received fields by comparison with a reference signal generator (derived from the exciter). In order to measure the ratio of received to transmitted field accurately, it is necessary to receive the transmitted pulse in the far field, delay it beyond the recovery time of the receivers, and retransmit this delayed signal through the radar receivers without losing coherence. The system for accomplishing this is shown in Fig. 5-5 for the sequential measurement system of Fig. 5-1. Part of the STALO signal is fed through an isolator to the radar antenna and transmitted to the antenna at the calibration site. Simultaneously, the calibration antenna receives the radar transmitted pulse. These two signals are mixed, giving a coherent i-f signal. This i-f signal is then amplified, and delayed in an i-f delay line. The delayed signal then is mixed with the received STALO signal and amplified in a traveling wave
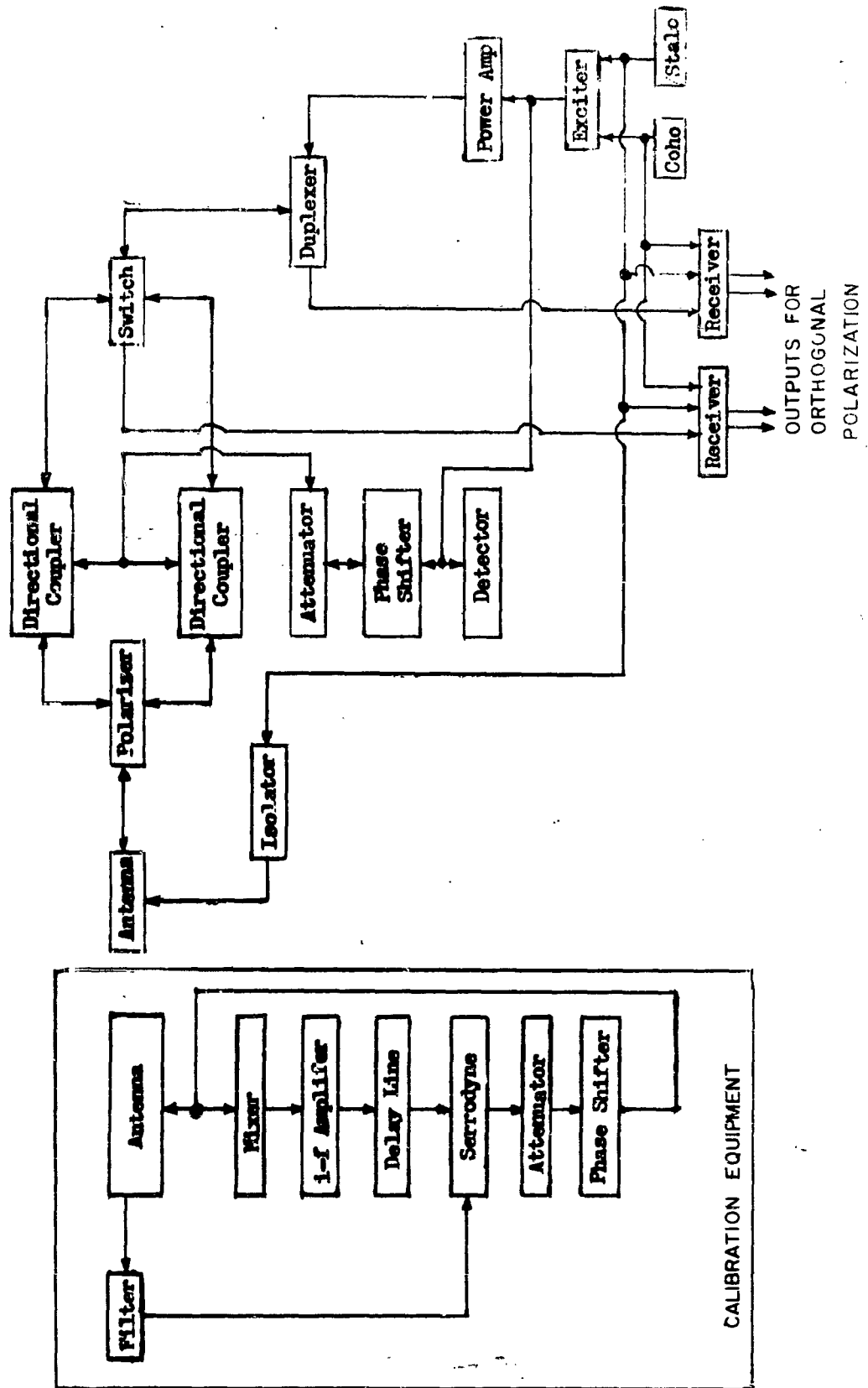
FIG. 5-5   RADAR BLOCK DIAGRAM   (SEQUENTIAL MEASUREMENTS)

80

tube, producing a delayed coherent pulse at the original transmitter frequency. This then is fed through an attenuator and phase shifter, and then re-radiated by the calibration antenna to the radar. It also returns, in part, through the mixer and delay line, giving rise to a second delayed pulse, and so on. Thus, a succession of pulses of constant amplitude ratio and phase difference is sent back to the radar. The attenuator and phase shifter in the calibration loop can be used to set the ratio of successive pulses at a desired value. For example, the amplitude ratio may be set at around 2 db in order to provide a large number of points on the receiver calibration curve.

The block diagram for the simultaneous system of Fig. 5-2 is shown in Fig. 5-6. For this system the calibration equipment has two circulating loops connected to the antenna through a diplexer. Also, two signal generator signals are obtained from the transmitter and compared in two detectors coupled to the receivers through a diplexer. Coherence between the two frequencies is obtained by use of a common STALO and COHO. The two sidebands of the exciter are thus coherent, so that measurements made on the two frequencies have a common phase reference once a calibration is performed to relate the phase at the exciter to the phase at the two reference detectors. The detectors will require good shielding to avoid interference during the measurement of the phase and amplitude of the transmitted pulse. A crystal detector and microammeter, properly packaged, should be suitable for this purpose. The details of the equipment will depend upon the particular application.

5.4.3 Typical System.

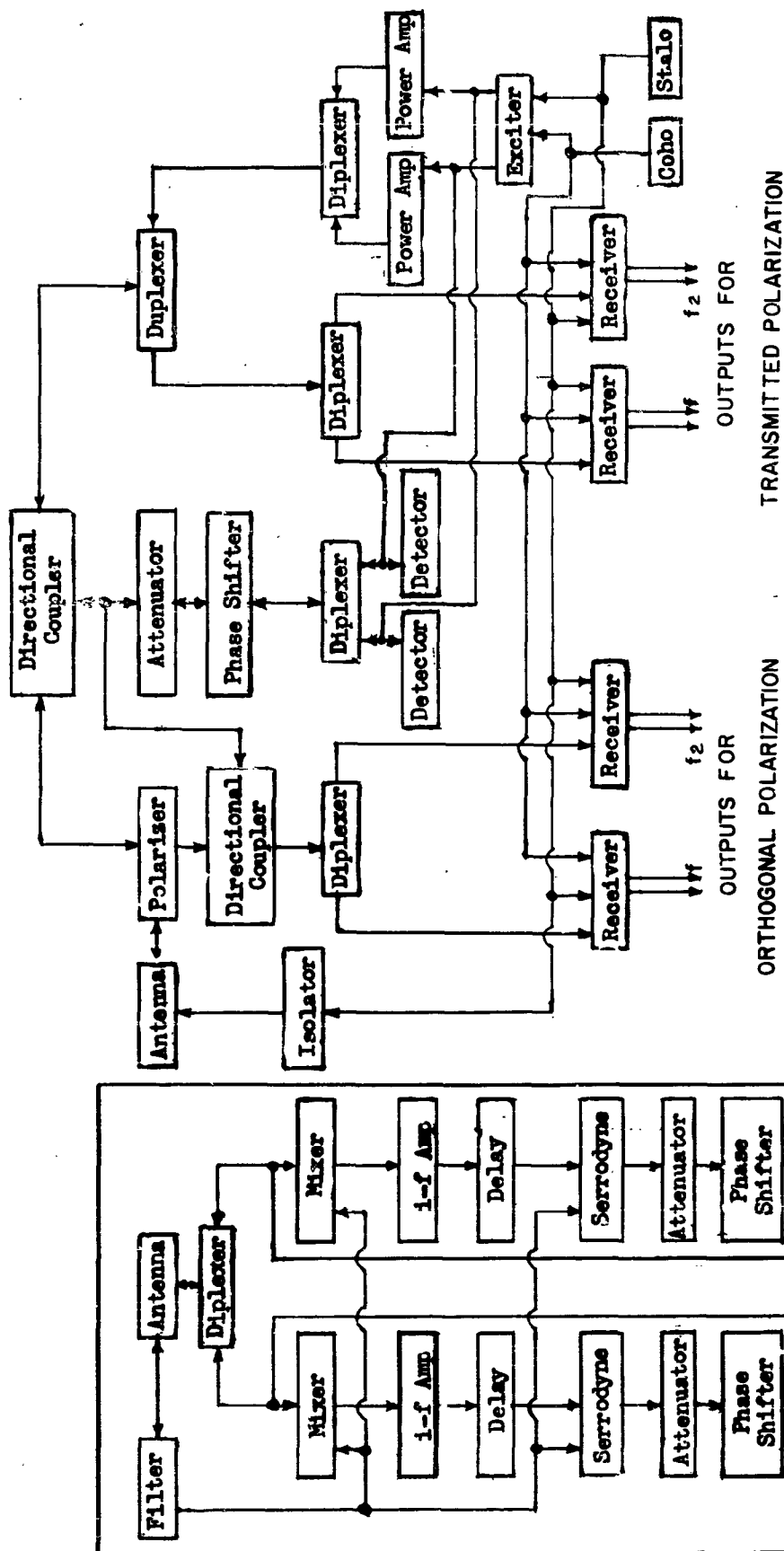The coherent radar measurement system has a number of potential

CALIBRATION EQUIPMENT

FIG. 5-6   RADAR BLOCK DIAGRAM (SIMULTANEOUS MEASUREMENTS)

82

applications. The recommended modifications of the Maynard field site radar for the measurement of ground clutter characteristics was described in detail in [1]. The essentials of such a design will be discussed here to give an illustration of its salient features.

A coherent pulsed search radar for the measurement of the radar length tensor for ground return (as described in [1]) is shown in the block diagram of Fig. 5-5. The COHO and STALO are mixed in a serrodyne exciter whose output is a 1 μs pulse with a peak power of 2.5 watts. The power amplifier has a peak power output of two megawatts at S-Band. The STALO has a short-time stability of one part in 10^8, which corresponds to a phase error in the measured radar length element of one degree for a target at a range of eight miles. The input of the receiver is a traveling wave tube amplifier with a narrow band pre-selector filter. The four simultaneous receiver outputs are recorded on magnetic tape for subsequent calculations. The calibration equipment is located in the far field of the radar antenna (about 2000 feet away). The delay line in the calibration equipment can separate successive pulses adequately if a delay of 2 μs is used. With radar and calibration antenna gains of 35 and 20 db respectively, the first calibration pulse will return to the radar 6 μs after the main bang at a level approximately 100 db above noise if the calibration loop loss is 2 db. Successive pulses will continue to appear at the radar for the next 100 μs to define a calibration curve with points separated in amplitude by 2 db and in phase by 7.2 degrees. The loop characteristics can be changed by adjusting the attenuator and phase shifter in the loop to give the number of calibration points desired.

By triggering the exciter, but not the power amplifier, at the appropriate time between transmitted pulses, a reference signal generator pulse is obtained

83

for mixing in the detector with either the transmitted pulse or one of the calibration pulses.

In operation, the radar is pointed toward the calibration equipment and the calibration information is recorded. The radar is then pointed at the area of ground to be measured and the ground return is recorded while the transmitter field is monitored to measure its stability. After the ground return measurement, the radar is again pointed toward the calibration equipment to obtain a calibration curve.

6. ARBITRARILY ORIENTED FACETS.

The computation of the back scattering from a random collection of rectangular facets of various sizes and slopes was considered in [7]. For depression angles which involve specular reflection from some of the facets (that is, some of the facets parallel to the wave front), in order to effect the resulting integrations it was necessary to assume that one edge of every facet was aligned with the wave front.

Since this assumption is somewhat artificial and specialized, an extension of the previous work to remove this restriction was investigated.

A large rectangular plate (facet) of width W and length L has a radar area

$$\sigma = \frac{1}{\pi}\left(k A \nu \frac{\sin X}{X}\frac{\sin Y}{Y}\right)^2 \tag{6.1}$$

where

$$X = k W l,$$

$$Y = k L \mu,$$

l, μ, ν being the direction cosines to the incident wave normal of the two edges and the normal of the facet, $A = WL$ is the area of the facet, and $k = 2\pi/\lambda$. If one edge is parallel to the wave front, then $l = 0$, so that the expression reduces to

$$\sigma = \frac{1}{\pi}\left(k A \nu \frac{\sin Y}{Y}\right)^2. \tag{6.2}$$

In considering the total radar area of an ensemble of randomly scattering facets having a pseudo-Gaussian distribution of orientations, (6.2) leads to the integral

$$I_1 = \frac{1}{\rho^2}\int_{-\infty}^{\infty} e^{-a^2\mu^2}\frac{\sin^2 \rho(c+b\mu)}{(c+b\mu)^2}\,d\mu. \tag{6.3}$$

The value of this integral was given in [7] as

85

$$I_1 = \frac{\pi e^{-y^2}}{2 a x^2}\left[z\, Erf(z) + z^* Erf(z^*) - i\, 2y\, Erf(iy) - \frac{2}{\sqrt{\pi}} e^{-x^2}(1 - x^2 \cos 2xy)\right] \quad (6.4)$$

where

$$z = x + iy = pb/a + i\, ac/b.$$

For a general orientation of the facet with respect to the wave normal, (6.1) leads to an integral of the type

$$I_2 = \frac{1}{P_1^2 P_2^2}\int_{-\infty}^{\infty} e^{-a^2 u^2}\frac{\sin^2 P_1(c_1 + b_1 u)}{(c_1 + b_1 u)^2}\frac{\sin^2 P_2(c_2 + b_2 u)}{(c_2 + b_2 u)^2}\, du, \quad (6.5)$$

where $P_1 = \frac{1}{2}W$, $P_2 = \frac{1}{2}L$, and the b's and c's are angular functions. This may be evaluated in the following way:

Writing $\mathcal{A} = P_1^2 P_2^2 I_2$, two-fold differentiation both with respect to P_1 and P_2 results in

$$\frac{\partial^4 \mathcal{A}}{\partial P_1^2 \partial P_2^2} = 4\int_{-\infty}^{\infty} e^{-a^2 x^2}\cos\{2 P_1(c_1 + b_1 u)\}\cos\{2 P_2(c_2 + b_2 u)\}\, du$$

$$= \frac{2\sqrt{\pi}}{a}\left[\cos(P_1 c_1 + P_2 c_2) e^{-\frac{(P_1 b_1 + P_2 b_2)^2}{a}} + \cos(P_1 c_1 - P_2 c_2) e^{-\frac{(P_1 b_1 - P_2 c_2)^2}{a}}\right]$$

Now successive indefinite integrations are performed, twice each with respect to P_1 and P_2. The constants of integration are determined at each stage by letting P_1 or P_2 go to zero, whereupon the integrated result should vanish. In this way, by a straightforward but tedious procedure, the following result is obtained:

$$I_2 = C \cdot Re\left\{ e^{-\left(\frac{c_2 a}{b_2}\right)^2}\left[F(z_1) + F(z_2) - 2F(z_3)\right]\right.$$

$$\left. - e^{-\left(\frac{c_1 a}{b_1}\right)^2}\left[F(z_4) + F(z_5) - 2F(z_6)\right]\right\}, \quad (6.6)$$

where

$$C = \frac{\pi a^4}{6 P_1^4 P_2^4 (c_2 b_1 - c_1 b_2)^2},$$

$$F(z_n) = f(z_n) - f(z_n^*),$$

$$F(z_n) = \left(z_n + \frac{1}{d_n}\right)e^{-d_n z_n} Erf(z_n) - \frac{1}{d_n}e^{-\frac{d_n^2}{4}} Erf\left(z_n + \frac{d_n}{2}\right) + \frac{1}{\sqrt{\pi}}e^{-(z_n^2 + d_n z_n)},$$

$$d_1 = d_2 = d_3 = -d_4 = -d_5 = -d_6 = i\,2a\left(\frac{c_2}{b_2} - \frac{c_1}{b_1}\right)$$

$$z_1 = \frac{P_1 b_1}{a} + \frac{P_2 b_2}{a} - i\,\frac{ac_2}{b_2}\,, \qquad\qquad z_1 + \frac{d_1}{2} = \frac{P_1 b_1}{a} + \frac{P_2 b_2}{a} - i\,\frac{ac_1}{b_1}$$

$$z_2 = \frac{P_1 b_1}{a} - \frac{P_2 b_2}{a} + i\,\frac{ac_2}{b_2}\,, \qquad\qquad z_2 + \frac{d_2}{2} = \frac{P_1 b_1}{a} - \frac{P_2 b_2}{a} - i\,\frac{ac_1}{b_1}$$

$$z_3 = \frac{P_1 b_1}{a} - i\,\frac{ac_2}{b_2} \qquad\qquad z_3 + \frac{d_3}{2} = \frac{P_1 \bar{b}_1}{a} - i\,\frac{ac_1}{b_1}$$

$$z_4 = \frac{P_2 b_2}{a} + \frac{P_1 b_1}{a} - i\,\frac{ac_1}{b_1} \qquad\qquad z_4 + \frac{d_4}{2} = \frac{P_2 b_2}{a} + \frac{P_1 b_1}{a} - i\,\frac{ac_2}{b_2}$$

$$z_5 = \frac{P_2 b_2}{a} - \frac{P_1 b_1}{a} - i\,\frac{ac_1}{b_1} \qquad\qquad z_5 + \frac{d_5}{2} = \frac{P_2 b_2}{a} - \frac{P_1 b_1}{a} - i\,\frac{ac_2}{b_2}$$

$$z_6 = \frac{P_2 b_2}{a} - i\,\frac{ac_1}{b_1} \qquad\qquad z_6 + \frac{d_6}{2} = \frac{P_2 b_2}{a} - i\,\frac{ac_2}{b_2}$$

$$z_1^o = \frac{P_2 b_2}{a} - i\,\frac{ac_2}{b_2} \qquad\qquad z_1^o + \frac{d_1}{2} = \frac{P_2 b_2}{a} - i\,\frac{ac_1}{b_1}$$

$$z_2^o = -\frac{P_2 b_2}{a} - i\,\frac{ac_2}{b_2} \qquad\qquad z_2^o + \frac{d_2}{2} = -\frac{P_2 b_2}{a} - i\,\frac{ac_1}{b_1}$$

$$z_3^o = -i\,\frac{ac_2}{b_2} \qquad\qquad z_3^o + \frac{d_3}{2} = -i\,\frac{ac_1}{b_1}$$

$$z_4^o = \frac{P_1 b_1}{a} - i\,\frac{ac_1}{b_1} \qquad\qquad z_4^o + \frac{d_4}{2} = \frac{P_1 b_1}{a} - i\,\frac{ac_2}{b_2}$$

$$z_5^o = -\frac{P_1 b_1}{a} - i\,\frac{ac_1}{b_1} \qquad\qquad z_5^o + \frac{d_5}{2} = -\frac{P_1 b_1}{a} - i\,\frac{ac_2}{b_2}$$

$$z_6^o = -i\,\frac{ac_1}{b_1} \qquad\qquad z_6^o + \frac{d_6}{2} = -i\,\frac{ac_2}{b_2}$$

(6.6) is the counterpart of (6.4) when the more general orientation is considered. (6.6) would be quite formidable to handle in the form above. But, since the dimensions of the facet are large, i.e., $\beta W \gg 1$, $\beta L \gg 1$, asymptotic expansions of the error functions may be employed. This is the same procedure used on (6.4) in [7]. (6.6) then reduces considerably in complexity, so that the remaining steps in the development may be carried out.

7. SUMMARY AND CONCLUSIONS.

A study of ground and sea clutter measurements, interpreted in the light of the results of theoretical investigations, indicates that the following physical mechanisms are of importance in scattering by ground surfaces:

(a) The plane-wave reflection coefficient of the surface (determined by its dielectric constant and conductivity);

(b) Reflection interference between direct and surface-reflected waves, which controls the illumination of the scattering elements;

(c) The aspect (slope) distribution of the scattering elements, which controls the angular variation of the scattering;

(d) The size distribution of the scattering elements, which controls the dependence of the scattering on frequency.

All of these mechanisms affect the polarization dependence of the scattering. In addition, the polarization dependence should be affected by the shape or form of the scattering elements.

An explanation of the polarization dependence of sea clutter appears to be available in terms of the polarization characteristics of small facets, together with the polarization characteristics of the reflection interference phenomenon at small depression angles. A comparable understanding of the polarization characteristics of ground clutter does not appear to be in hand.

Coherent radar systems described in this report, together with a new quantitative calibration technique which has been devised, are especially suited for making measurements of the complete radar polarization characteristics of ground targets.

88

8. - RECOMMENDATIONS.

On the basis of the mechanisms and characteristics revealed by clutter measurements, the following recommendations are submitted:

(a) A program of extensive measurements of the polarization characteristics of various types of areas should be undertaken. Specific recommendations for such a program in connection with the radar at the Maynard field site already have been submitted [1].

(b) Theoretical investigations of the polarization characteristics of typical forms of scattering elements should be continued. These results should then be applied in the interpretation of experimental measurements arising from (a) above.

(c) Analysis of existing clutter measurements should be continued, with the goal of attaining a complete quantitative understanding of the phenomena.

9. REFERENCES.

[1] E. A. Wolff, "A program for the measurement of ground clutter", Electro-
magnetic Research Corporation, Report No. CRC-5198-1, Contract No.
AF19(604)-5198, December 21, 1959.

[2] L. M. Spetner & I. Katz, "Further analysis of radar terrain return",
The John Hopkins University Applied Physics Laboratory, Report
APL/JHU CF-2843, 10 November, 1959.

[3] F. C. Macdonald, " The correlation of radar sea clutter on vertical and
horizontal polarization with wave height and slope", IRE Convention
Record, vol. 4, Part 1, pp. 29-32, 1956.

[4] D. E. Kerr, Ed., "Propagation of Radio Waves", M.I.T. Radiation Lab.
Ser., McGraw-Hill Book Co., Inc., New York, N.Y., vol. 13, pp.
481-587, 1951.

[5] H. Goldstein, "Frequency dependence of the properties of sea echo",
Phys. Rev., vol. 70, pp. 938-946, December 1 and 15, 1946.

[6] M. Katzin, "On the mechanisms of radar sea clutter", Proc. IRE., v. 45,
pp. 44-54, Jan. 1957.

[7] M. Katzin, "Sea clutter at large depression angles", Final report on
Contract NOnr-2138(00), Oct. 12, 1958, ASTIA AD 225 599.

[8] C. R. Grant and B. S. Yaplee, "Back scattering from water and land at
centimeter and millimeter wavelengths", Proc. IRE, vol. 45, pp.
976-982, July 1957.

[9] Anon, "Measurements of terrain back-scattering coefficients with an
airborne X-band radar", Goodyear Aircraft Corporation, Report
GERA-463, 30 September 1959.

[10] S. O. Rice, " Reflection of electromagnetic waves by slightly rough surfaces", Comm. on Pure and App. Math., vol. IV, pp. 351-378, 1951.

[11] W. H. Peake, "Theory of radar return from terrain", IRE National Convention Record, vol. 7, Part 1, pp. 27-44, 1959.

[12] R. C. Taylor, "Terrain return measurements at X, K_u and K_a band", IRE National Convention Record, vol. 7 part 1, pp. 19-26, 1959.

[13] H. G. Booker, "Slot aerials and their relation to complementary wire aerials (Babinet's principle)", J. IEE, vol. 93, part IIIA, pp. 620-626, 1946.

[14] E. T. Copson, "An integral-equation method of solving plane diffraction problems", Proc. Roy. Soc. (A), vol. 186, pp. 100-118, June 4, 1946.

[15] H. A. Bethe, "Theory of diffraction by small holes", Phys. Rev., vol. 66, pp. 163-182, October 1 and 15, 1944.

[16] C. J. Bouwkamp, "On Bethe's theory of diffraction by small holes", Philips Research Reports, vol. 5, pp. 321-332, October 1950.

[17] J. Meixner and W. Andrejewski, "Strenge Theorie der Beugung ebener elektromagnetischer Wellen an der vollkommen leitenden Kreisscheibe und an der kreisförmigen Öffnung in vollkommen leitenden ebenen Schirm", Ann. d. Phys. (6), vol. 7, pp. 157-168, April 1950.

[18] C. Flammer, "The vector wave function solution of the diffraction of electromagnetic waves by circular disks and apertures. II. The diffraction problems", Jour. App. Phys., vol. 24, pp. 1224-1231, Sept. 1953.

[19] B. Y.-C. Koo and M. Katzin, "An exact earth-flattening procedure in propagation around a sphere", Jour. Res. NBS, vol. 64D, pp. 61-64, Jan.-Feb, 1960.

[20] E. Kennaugh, "Techniques for echo area determination", Ohio State University Antenna Laboratory, Report No. 792-5, 1 Februar Contract No. AF33(616)-5398, ASTIA Document No. AD 211 860

[21] D. L. Ringwalt, "A model technique for the measurement of the re characteristics of targets", Naval Research Laboratory Rep No. 3800, June 29, 1951.

[22] D. L. Ringwalt, "An airborne radar and wave propagation laborat IRE Convention Record, vol. 3, Part 1, pp. 82-85, 1955.

[23] B. E. Gorr, "Air Force Cambridge Research Center radar cross se measuring equipment and range", AFCRC Technical Report TR- April 1959.

[24] A. J. Simmons & H. N. Chait, "Arbitrarily polarized antennas for S-, and L-bands", Naval Research Laboratory Report No. 39 May 1, 1952.

[25] M. Katzin, "Quantitative radar measurements", Proc. IRE, vol. 35 p. 1333, Nov. 1947.

[26] E. A. Wolff, "A method of making a radar self-calibrating", Pr vol. 42, pp. 1522-1526, Oct. 1954.